

MARK4 controls ischaemic heart failure through microtubule detyrosination

<https://doi.org/10.1038/s41586-021-03573-5>

Received: 15 December 2019

Accepted: 21 April 2021

Published online: 26 May 2021

 Check for updates

Xian Yu^{1,12}, Xiao Chen^{2,12}, Mamta Amrute-Nayak³, Edward Allgeyer^{4,5}, Aite Zhao⁶, Hannah Chenoweth¹, Marc Clement¹, James Harrison¹, Christian Doreth¹, George Sirinakis^{4,5}, Thomas Krieg⁷, Huiyu Zhou⁸, Hongda Huang⁹, Kiyotaka Tokuraku¹⁰, Daniel St Johnston^{4,5}, Ziad Mallat^{1,11} & Xuan Li¹✉

Myocardial infarction is a major cause of premature death in adults. Compromised cardiac function after myocardial infarction leads to chronic heart failure with systemic health complications and a high mortality rate¹. Effective therapeutic strategies are needed to improve the recovery of cardiac function after myocardial infarction. More specifically, there is a major unmet need for a new class of drugs that can improve cardiomyocyte contractility, because inotropic therapies that are currently available have been associated with high morbidity and mortality in patients with systolic heart failure^{2,3} or have shown a very modest reduction of risk of heart failure⁴. Microtubule detyrosination is emerging as an important mechanism for the regulation of cardiomyocyte contractility⁵. Here we show that deficiency of microtubule-affinity regulating kinase 4 (MARK4) substantially limits the reduction in the left ventricular ejection fraction after acute myocardial infarction in mice, without affecting infarct size or cardiac remodelling. Mechanistically, we provide evidence that MARK4 regulates cardiomyocyte contractility by promoting phosphorylation of microtubule-associated protein 4 (MAP4), which facilitates the access of vasohibin 2 (VASH2)—a tubulin carboxypeptidase—to microtubules for the detyrosination of α -tubulin. Our results show how the detyrosination of microtubules in cardiomyocytes is finely tuned by MARK4 to regulate cardiac inotropy, and identify MARK4 as a promising therapeutic target for improving cardiac function after myocardial infarction.

Myocardial infarction—the main cause of ischaemic heart disease and chronic heart failure—is a serious ischaemic syndrome in which the blood supply to the heart is blocked, thus causing substantial death of myocardial cells and loss of function in the remaining viable cells⁶. Microtubule detyrosination, which is associated with desmin at force-generating sarcomeres⁵, is upregulated in failing hearts of patients with ischaemic cardiomyopathy^{5,7} and hypertrophic cardiomyopathies^{5,7,8}, and suppression of microtubule detyrosination improves contractility in failing cardiomyocytes⁷. VASH1 or VASH2, coupled to a small vasohibin-binding protein (SVBP), forms tubulin carboxypeptidases (TCPs) that are capable of tubulin detyrosination^{9,10}. Depletion of VASH1 increases the speed of contraction and relaxation in failing human cardiomyocytes¹¹. Structural and biophysical studies have suggested that VASH interacts with the C-terminal tail of α -tubulin^{12–14}. However, the regulatory mechanisms of this system are still poorly understood.

Microtubule stability is regulated by microtubule-associated proteins (MAPs), including classical MAPs such as MAP2, MAP4 and tau¹⁵. MAP4 is expressed in cardiomyocytes and the level of MAP4

significantly increases in human hearts with cardiomyopathy⁷. MAP4 dephosphorylation on the microtubule network has previously been described in a feline model of pressure-overload cardiac hypertrophy¹⁶, but the relationship between MAP4 phosphorylation and microtubule detyrosination has not been examined. MARK4 is an evolutionarily conserved serine–threonine kinase^{17,18} that is known to phosphorylate MAPs including tau, MAP2 and MAP4, on KXGS motifs within their microtubule-binding repeats^{19–21}. The phosphorylation of MAPs triggered by MARK induces conformational changes that alter the association of MAPs with microtubules, and thereby regulates microtubule dynamics^{19–21}. MARK4 is expressed in the heart²⁰, however, the role of MARK4 in the cardiomyocyte has not been studied. Here we examined whether MARK4 regulates the function of the failing cardiomyocyte through modulation of microtubule detyrosination.

Function of *Mark4*^{−/−} hearts after myocardial infarction

To evaluate the effect of MARK4 in the setting of ischaemic heart disease, we used a mouse model of permanent left anterior descending

¹Department of Medicine, Cardiovascular Division, University of Cambridge, Addenbrooke's Hospital, Cambridge, UK. ²Department of Cardiology, Union Hospital, Tongji Medical College, Huazhong University of Science and Technology, Wuhan, China. ³Department of Molecular and Cell Physiology, Hannover Medical School, Hannover, Germany. ⁴The Gurdon Institute, University of Cambridge, Cambridge, UK. ⁵Department of Genetics, University of Cambridge, Cambridge, UK. ⁶College of Computer Science and Technology, Qingdao University, Shandong, China. ⁷Department of Medicine, Experimental Medicine and Immunotherapeutics Division, University of Cambridge, Addenbrooke's Hospital, Cambridge, UK. ⁸School of Informatics, University of Leicester, Leicester, UK. ⁹Department of Biology, Southern University of Science and Technology, Shenzhen, China. ¹⁰Muroran Institute of Technology, Muroran, Japan.

¹¹Université de Paris, Institut National de la Santé et de la Recherche Médicale, U970, PARCC, Paris, France. ¹²These authors contributed equally: Xian Yu, Xiao Chen. ✉e-mail: XL315@cam.ac.uk

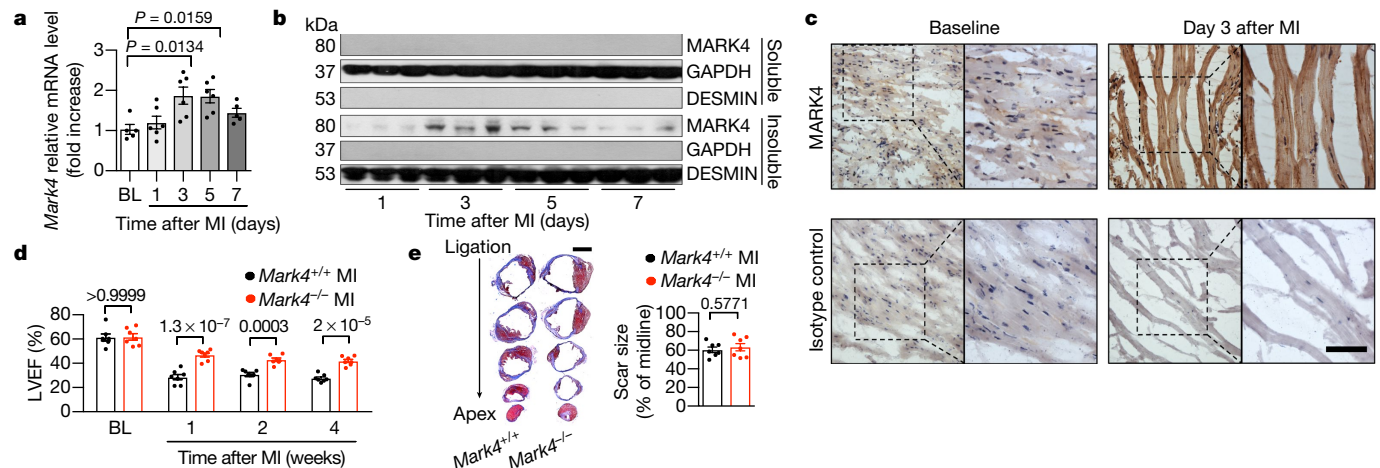


Fig. 1 | MARK4 deficiency preserves cardiac function after myocardial infarction without altering the size of the scar. **a**, Expression of *Mark4* mRNA in heart samples from wild-type hearts, baseline hearts (BL; hearts without myocardial infarction) and from hearts obtained at the indicated days (1, 3, 5 and 7 days) after myocardial infarction (MI) was analysed using real-time PCR. $n=5$ at baseline, $n=6$ mice per time point at 1, 3 and 5 days after myocardial infarction and $n=5$ mice at 7 days after myocardial infarction. **b**, Western blots of MARK4 in the insoluble cytoskeletal fractions (with desmin as marker) and GAPDH in corresponding soluble cytosolic fractions is shown. $n=3$ mice at each time

point. **c**, Representative immunohistochemistry staining of MARK4 in wild-type mice at baseline or after myocardial infarction. Isotype IgG was used as control. Scale bar, 50 μ m. **d**, Assessment of LVEF in *Mark4^{-/-}* mice ($n=7$) and their littermate controls (*Mark4^{+/+}*) ($n=7$) at baseline, and 1, 2 and 4 weeks after myocardial infarction. **e**, Scar size at week 4 after myocardial infarction. Scale bar, 2 mm. **a, d, e**, Data are mean \pm s.e.m. One-way analysis of variance (ANOVA) with Bonferroni post hoc correction (a); two-way ANOVA with Bonferroni post hoc correction for multiple comparisons (d); two-tailed unpaired Student's *t*-test (e). *P* values are indicated.

coronary artery ligation to induce a large myocardial infarction^{22,23} (Extended Data Fig. 1a). We detected *Mark4* mRNA (Fig. 1a) and MARK4 protein (Fig. 1b) expression in the heart tissues, peaking between day 3 and day 5 after myocardial infarction (Fig. 1a–c). MARK4 was almost exclusively detected in the cytoskeleton-enriched insoluble fraction of the whole-heart extracts (Fig. 1b) and was localized in cardiomyocytes (Fig. 1c and Extended Data Fig. 2a). MARK4-deficient mice (*Mark4^{-/-}*) displayed a remarkable preservation of left ventricular ejection fraction (LVEF), which was 63.6% (\pm 5.8%) higher compared with their wild-type littermate controls on the first week after left anterior descending coronary artery ligation (Fig. 1d), without any alteration in cardiac remodelling (Supplementary Table 1). Notably, infarct scar size was similar between the two groups of mice (Fig. 1e), indicating that the substantial difference in cardiac function between wild-type and *Mark4^{-/-}* mice was not attributable to differences in the size of viable cardiac tissues.

MARK4 regulates cardiac contractility

We found that the protective effect of MARK4 deficiency on the preservation of cardiac function was already apparent at 24 h after myocardial infarction (Fig. 2a and Extended Data Fig. 1b), despite a similar extent of myocardial injury, shown by comparable serum levels of cardiac troponin I (Fig. 2b) and a comparable infarct size analysed by triphenyltetrazolium chloride staining (Fig. 2c), in *Mark4^{-/-}* and wild-type mice. MARK4 has previously been shown to regulate NLRP3 activation in macrophages^{24,25}, which could affect the outcome of a post-ischaemic injury given the role of the NLRP3 inflammasome in this setting^{26,27}. However, MARK4 deficiency did not significantly alter local and systemic inflammatory responses to myocardial injury at day 3 after myocardial infarction (Extended Data Fig. 2b and Supplementary Table 2) when the preservation of the LVEF was already evident in *Mark4^{-/-}* mice (Extended Data Fig. 2c). Moreover, bone marrow transfer of *Mark4^{-/-}* haematopoietic cells into wild-type mice (Extended Data Fig. 1c; validation in Extended Data Fig. 3a, b) did not improve cardiac function after myocardial infarction in comparison with the transfer of wild-type bone marrow cells (Fig. 2d), indicating that the protective

effect of MARK4 deficiency after myocardial infarction could not be explained by the role of MARK4 in haematopoietic cells. By contrast, using an inducible conditional deletion of *Mark4* in cardiomyocytes (*Mark4* conditional knockout (cKO)) (Extended Data Fig. 1d; validation in Extended Data Fig. 3c), we found a substantial preservation of LVEF in *Mark4* cKO mice after myocardial infarction, which was 56.8% (\pm 6.2%) higher compared with littermate control mice at day 1 after myocardial infarction (Fig. 2e). The protective effect seen in *Mark4* cKO mice started as early as the first day after myocardial infarction and lasted until the end of the observation at four weeks after myocardial infarction (Fig. 2e). Notably, *Mark4* cKO mice had a reduction of only 4.3% (\pm 3.8%) in LVEF at day 1 after myocardial infarction, compared with a reduction of 37.9% (\pm 5.5%) in the control mice (Fig. 2e), without any difference in infarct size (Extended Data Fig. 3e). The data further show that the remaining, viable MARK4-deficient cardiomyocytes affect contractile function. Collectively, our data demonstrate that cardiomyocyte-expressed MARK4 has an intrinsic role in the control of cardiac function after myocardial infarction.

To examine the effect of MARK4 on cardiomyocyte function, we subjected freshly isolated primary cardiomyocytes²⁸ from wild-type and *Mark4^{-/-}* mice to a single-cell contractility assay using an electrical stimulator (Fig. 2f–i). We found that sarcomere peak shortening of isolated cardiomyocytes strongly correlated with the *in vivo* LVEF (Fig. 2f), indicating that the contraction of isolated cardiomyocyte measured *ex vivo* reflects LVEF assessed *in vivo* (Figs. 1d, 2a, e). At baseline, wild-type and MARK4-deficient cardiomyocytes had similar levels of resting sarcomere length (Extended Data Fig. 4a, b), sarcomere peak shortening and contraction and relaxation velocities (Fig. 2g–i), an observation that is consistent with the absence of a difference in LVEF between wild-type and *Mark4^{-/-}* mice before myocardial infarction (Fig. 1d). After myocardial infarction, wild-type cardiomyocytes displayed markedly reduced sarcomere shortening (decreased by 22.5% \pm 3.7%) (Fig. 2g and Extended Data Fig. 4c), with slower relaxation velocity (decreased by 25.2% \pm 4.4%) (Fig. 2i and Extended Data Fig. 4e), compared with cardiomyocytes isolated from wild-type mice without myocardial infarction. Notably, although no difference in resting sarcomere length

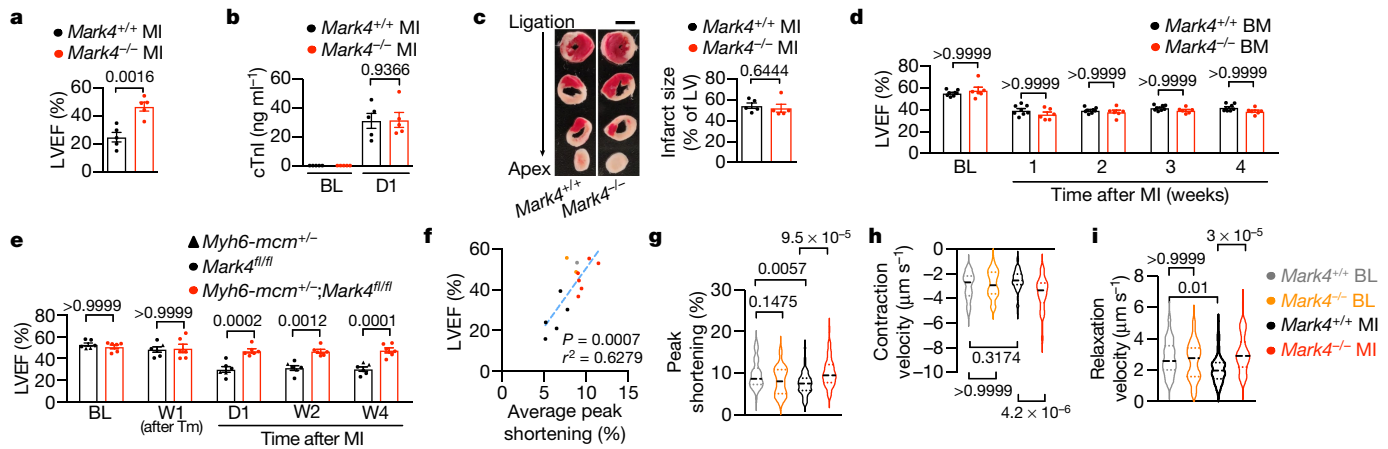


Fig. 2 | MARK4 expression in cardiomyocytes regulates cardiac contractile function after myocardial infarction. **a–c**, *Mark4*^{-/-} mice ($n=5$) and their littermate controls (*Mark4*^{+/+}, $n=5$) at day 1 (D1) after myocardial infarction. **a**, LVEF. **b**, **c**, Circulating cardiac troponin I (cTnI) levels (**b**) and infarct size (**c**) at 24 h after myocardial infarction are shown. Cardiac troponin I measurements at baseline were used as controls. Scale bar, 2 mm. **d**, Assessment of LVEF in chimeric mice ($n=8$ wild-type recipients of *Mark4*^{+/+} bone marrow (BM) donors; $n=6$ wild-type recipients of *Mark4*^{-/-} bone marrow donors) at the indicated time points. **e**, Assessment of LVEF at the indicated time points after conditional *Mark4* knockout using tamoxifen (Tm) in *Myh6-mcm*^{+/+}; *Mark4*^{fl/fl} (also known as α MHC-*mcm*^{+/+}; *Mark4*^{fl/fl}) mice ($n=6$) (*Myh6* encodes the cardiomyocyte-specific marker α MHC). Tamoxifen-injected *Myh6-mcm*^{+/+} and *Mark4*^{fl/fl} littermate mice were used as controls ($n=6$). **f–i**, Contractility assay of single primary cardiomyocytes isolated at baseline or at day 3 after myocardial

infarction in the following groups: baseline, *Mark4*^{+/+} mice ($n=4$ mice, $n=45$ cardiomyocytes examined over 4 independent experiments); baseline, *Mark4*^{-/-} mice ($n=3$ mice, $n=45$ cardiomyocytes examined over 3 independent experiments); myocardial infarction, *Mark4*^{+/+} mice ($n=5$ mice, $n=54$ cardiomyocytes examined over 5 independent experiments); and myocardial infarction, *Mark4*^{-/-} mice ($n=6$ mice, $n=57$ cardiomyocytes examined over 6 independent experiments). **f**, Correlation between LVEF (measured at day 1 after myocardial infarction) and sarcomere peak shortening. **g**, Sarcomere peak shortening. **h**, **i**, Pooled data of contraction (**h**) and relaxation (**i**) velocity. **a–e**, Data are mean \pm s.e.m. **g–i**, Violin plots show lines at the median (solid) and quartiles (dashed). Two-tailed unpaired *t*-test (**a–c**); two-way ANOVA with Bonferroni post hoc correction for multiple comparisons (**d, e, g–i**). *P* values are indicated.

was observed between *Mark4*^{-/-} and wild-type cardiomyocytes after myocardial infarction (Extended Data Fig. 4b). *Mark4*^{-/-} cardiomyocytes displayed a greater level of sarcomere shortening (increased by $36.0\% \pm 6.0\%$) (Fig. 2g and Extended Data Fig. 4d) together with a greater velocity during both the contraction (increased by $42.0\% \pm 6.9\%$) and relaxation (increased by $46.7\% \pm 7.5\%$) phases (Fig. 2h, i and Extended Data Fig. 4f) compared with wild-type cardiomyocytes. Upstream changes in the influx of calcium (Ca^{2+}) through excitation–contraction coupling could contribute to the contractile alterations; however, we did not observe any significant difference in Ca^{2+} transients between electrically stimulated *Mark4*^{-/-} and wild-type cardiomyocytes at baseline or at day 3 after myocardial infarction (Extended Data Fig. 4g–m). These data demonstrate that *MARK4* deficiency substantially improves both contractile and relaxation functions of cardiomyocytes after myocardial infarction.

MARK4 alters microtubule dytrosination

Detyrosinated microtubules represent tunable, compression-resistant elements that impair cardiac function in failing hearts in humans^{5,7}. We confirmed that the level of detyrosinated α -tubulin was significantly higher in cardiomyocytes isolated from ischaemic hearts compared with cardiomyocytes isolated from mice that received a sham operation, in contrast to the remaining cell pool (immune cells, fibroblasts and endothelial cells), which did not display a change in α -tubulin detyrosination (Extended Data Fig. 2d, e). Previous data indicated that MARK4 affects the posttranslational detyrosination and polyglutamylation of microtubules in ciliated cells²⁹. Therefore, we hypothesized that MARK4 deficiency may affect microtubule detyrosination in cardiomyocytes after myocardial infarction. We found a significantly lower level of detyrosinated microtubules in whole-heart tissue extracts (Fig. 3a, b), and in isolated cardiomyocytes (together with reduced polyglutamylated microtubules) (Fig. 3e–g and Extended Data Fig. 2f, g) of *Mark4*^{-/-} mice compared with littermate wild-type controls after

myocardial infarction. In the absence of MARK4, we observed a reduced ratio of α -tubulin in the soluble fraction versus its level in the insoluble fraction (Fig. 3c), indicating a reduced percentage of free tubulin without MARK4. Notably, we found that the level of tubulin detyrosination inversely correlated with LVEF (Fig. 3d), suggesting that the MARK4-dependent modulation of microtubule detyrosination has an important role in controlling cardiac function after myocardial infarction.

To further address the hypothesis that MARK4 deficiency improves cardiomyocyte contractility through its influence on microtubule detyrosination, we used a genetic approach to overexpress tubulin tyrosine ligase (TTL) using an adenovirus system (Extended Data Fig. 5a–c) to reverse the effect of TCP³⁰ (Fig. 3h–j). TTL overexpression robustly improved peak shortening (Fig. 3h and Extended Data Fig. 5d) and increased the velocity of both contraction and relaxation (Fig. 3i, j and Extended Data Fig. 5g) of failing wild-type cardiomyocytes⁷. However, overexpression of TTL could not further improve peak shortening (Fig. 3h and Extended Data Fig. 5e) and contractile velocities of *Mark4*^{-/-} cardiomyocytes after myocardial infarction (Fig. 3i, j and Extended Data Fig. 5h), which is consistent with the already low level of detyrosinated microtubules in *Mark4*^{-/-} cardiomyocytes. We further confirmed these data using a pharmacological approach with parthenolide to inhibit microtubule detyrosination^{5,7} (Extended Data Fig. 5j–s). Taken together, our data show that MARK4 regulates cardiac inotropic function through its effect on microtubule detyrosination in cardiomyocytes.

MARK4 directs VASH2 access to microtubules

Detyrosination of α -tubulin preferentially occurs on polymerized microtubules³¹. Apart from binding to VASH, the C-terminal tubulin tails of polymerized microtubules are also important for MAP binding^{32,33}. MAP4 bound to the C-terminal tubulin tail along the protofilament stabilizes the longitudinal contacts of the microtubule, and this interaction can affect other microtubule-binding partners such as the motor

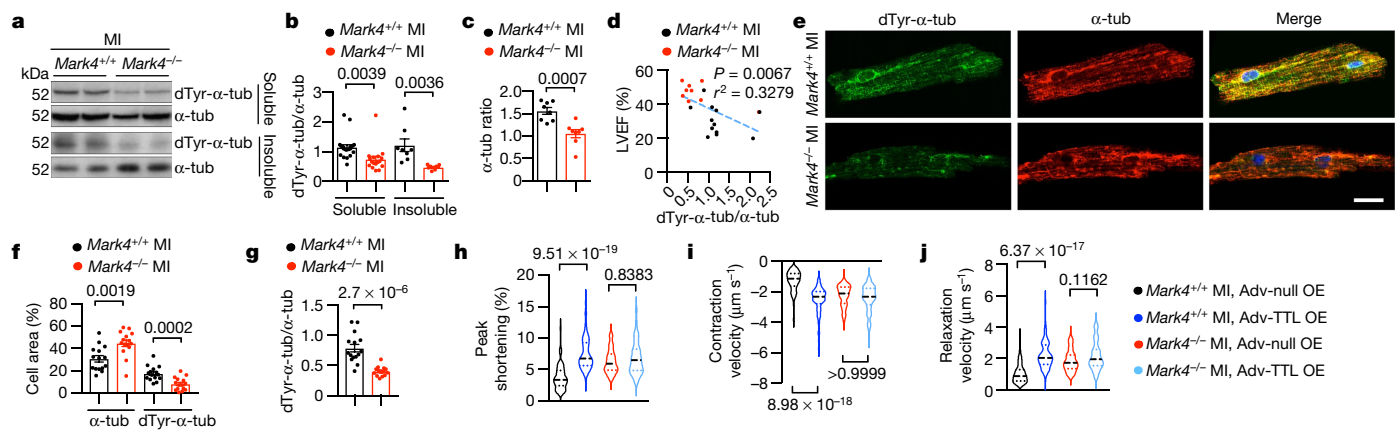


Fig. 3 | MARK4 regulates cardiomyocyte contractility by promoting microtubule detyrosination. **a–d**, Western blots of whole-heart extraction from mice at day 3 after myocardial infarction, in soluble and insoluble fractions. dTyr-tub, detyrosinated α -tubulin; α -tub, α -tubulin.

a, Representative western blots. **b**, Ratio of detyrosinated α -tubulin over total α -tubulin in the following groups: myocardial infarction, soluble fraction, $Mark4^{+/+}$ mice ($n=20$); myocardial infarction, soluble fraction, $Mark4^{-/-}$ mice ($n=17$); myocardial infarction, insoluble fraction, $Mark4^{+/+}$ mice ($n=8$); and myocardial infarction, insoluble fraction $Mark4^{-/-}$ mice ($n=8$). **c**, Ratio of α -tubulin in the soluble fraction over α -tubulin in the insoluble fraction ($n=8$ mice per group). **d**, Correlation between LVEF and the ratio of detyrosinated α -tubulin/ α -tubulin in $Mark4^{-/-}$ ($n=9$) and control mice ($n=12$). **e–g**, Confocal images of isolated cardiomyocytes at day 3 after myocardial infarction. **e**, Representative images. Scale bar, 20 μ m. **f**, **g**, Percentage of detyrosinated α -tubulin or total α -tubulin area per cell (**f**) and ratio of detyrosinated α -tubulin/total α -tubulin ($n=3$ mice, $n=15$ cardiomyocytes per

group) (**g**). **h–j**, Adenovirus (Adv)-mediated overexpression (OE) of TTL in primary cardiomyocytes isolated from $Mark4^{-/-}$ or control mice at day 3 after myocardial infarction, with overexpression of a null virus as controls. Contractility assay of single cardiomyocytes in the following groups: myocardial infarction, Adv-Null, $Mark4^{+/+}$ mice ($n=3$ mice, $n=75$ cardiomyocytes examined over 3 independent experiments); myocardial infarction, Adv-TTL, $Mark4^{+/+}$ mice ($n=3$ mice, $n=69$ cardiomyocytes examined over 3 independent experiments); myocardial infarction, Adv-Null, $Mark4^{-/-}$ mice ($n=3$ mice, $n=74$ cardiomyocytes examined over 3 independent experiments); and myocardial infarction, Adv-TTL, $Mark4^{-/-}$ mice ($n=3$ mice, $n=73$ cardiomyocytes examined over 3 independent experiments). **h**, Sarcomere peak shortening. Pooled data of contraction (**i**) and relaxation (**j**) velocity. **h–j**, Violin plots show lines at the median (solid) and quartiles (dashed). **b, c, f, g**, Data are mean \pm s.e.m. Two-tailed unpaired t-test (**b, c, f, g**); two-tailed correlation test (**d**); two-way ANOVA with Bonferroni post hoc correction for multiple comparisons (**h–j**). *P* values are indicated.

protein kinesin-1³³. MARK4, as a kinase, is expected to phosphorylate MAP4 at its KXGS motifs (including S941 and S1073 in human MAP4, or S914 and S1046 in mouse MAP4) within its microtubule-binding repeats^{19,20} (Extended Data Fig. 6a) and alter MAP4-binding status on the protofilament (Extended Data Fig. 6b). We therefore hypothesized that MARK4—by modifying MAP4 phosphorylation—may affect VASH accessibility to the C-terminal α -tubulin tail and therefore influence microtubule detyrosination. As such, we used an in vitro microtubule co-sedimentation assay. Both MAP4 (Extended Data Fig. 6c, d) and VASH2-SVBP (Extended Data Fig. 6e, f) were able to incrementally bind to polymerized microtubules when incremental amounts were separately applied in the assays, which is consistent with the results of previous studies^{12,33}. Notably, we found that VASH2-SVBP bound to polymerized microtubules gradually decreased in the presence of incremental amounts of previously bound MAP4 (with four microtubule-binding repeats (4R-MAP4)) (Fig. 4a, b). Therefore, these results support the hypothesis that the level of MAP4 occupancy on the polymerized microtubules influences the level of access of VASH2 to the microtubule protofilaments.

To confirm this hypothesis in vivo, we performed biochemical subcellular fractionation on primary cardiomyocytes isolated from non-ischaemic and ischaemic hearts of wild-type and $Mark4^{-/-}$ mice using a commercial kit, which we have validated (Extended Data Fig. 7a, b). We first confirmed that MAP4 was expressed in the cardiomyocytes and that the level of MAP4 was higher after myocardial infarction (Extended Data Fig. 7c), a result consistent with data showing that MAP4 levels significantly increase in hearts of individuals with cardiomyopathies⁷. MAP4 was detected in its S914 phosphorylated form ((pMAP4(S914); S914 is located within the KXGS motif) in the pellet extraction buffer (PEB) and also in its S1046 form (pMAP4(S1046); S1046 is located within the KXGS motif) in the cytosolic extraction buffer (CEB) (Extended Data Fig. 7c–e). Knocking down MAP4 using small hairpin RNA (shRNA) in isolated cardiomyocytes after myocardial infarction led to increased

VASH2 levels in the PEB fraction, which was confirmed by both western blot and immunocytochemistry (Extended Data Fig. 7f–i); these results are in line with the results of an in vitro microtubule co-sedimentation assay (Fig. 4a, b). VASH2 was detected as a specific band (validated by specific knockdown using shRNA) (Extended Data Fig. 8a) of around 50 kDa in the PEB fraction (Extended Data Fig. 8a, b), which is higher than its theoretical molecular weight of 40 kDa and presumably due to the formation of a stable complex with SVBP, because the addition of a denaturing agent (urea) reduced its size to around 40 kDa (Extended Data Fig. 8b). After myocardial infarction, pMAP4(S914) was detected in a 110 kDa form in the PEB fraction whereas pMAP4(S1046) was detected in a 220 kDa form in the CEB fraction (Fig. 4c and Extended Data Fig. 7c). MAP4 was detected as giant puncta in the cytosol of cardiomyocytes isolated after myocardial infarction, and these puncta were barely present at baseline (Extended Data Fig. 8c, d). pMAP4(S1046) (in the CEB fraction) formed oligomerized structures (at 440 kDa or higher) as revealed by native gel analysis (Extended Data Fig. 8e, f), and these pMAP4(S1046) oligomers could be further reduced to the 220 kDa form in the presence of urea as revealed by denaturing gel analysis (Extended Data Fig. 8g). The data suggest that MAP4 phosphorylation at S1046 is associated with its presence as oligomers or giant puncta in the cytosol in situ. Our results are consistent with a structural model, in which S914 is within the weak binding site of the microtubule-binding repeat of MAP4 to the microtubules, whereas S1046 is within the strong anchor point of the microtubule-binding repeat of MAP4 to the microtubules³³ (Extended Data Fig. 6b), so that phosphorylation at S1046 leads to the detachment of MAP4 from polymerized microtubules and accumulation in the cytosol. Accordingly, a higher level of pMAP4(S1046) was strongly and positively correlated with increased VASH2 levels in the PEB fraction (there was also a weaker correlation between pMAP4(S914) levels and VASH2 levels in the PEB fraction) (Extended Data Fig. 7c, e) in wild-type cardiomyocytes, indicating an association between pMAP4 (phosphorylated at S914 and S1046) and VASH2 levels on

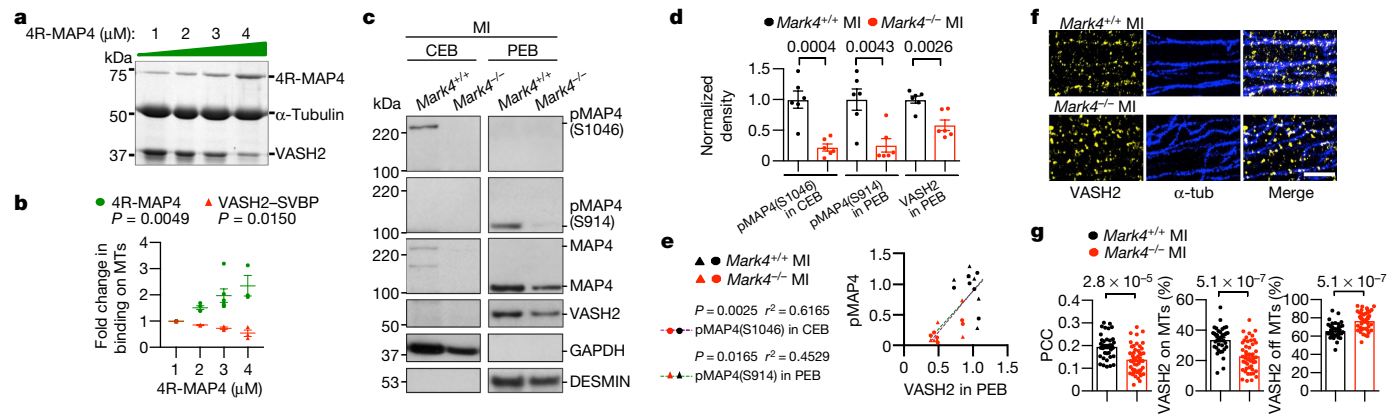


Fig. 4 | MARK4 controls microtubule detyrosination through MAP4 phosphorylation to facilitate VASH2 access to microtubules. **a, b,**

Representative gel image of VASH2-SVBP (3 μM) binding to polymerized microtubules (MTs) (5 μM) in the presence of different amounts of 4R-MAP4 (1–4 μM) in a microtubule co-sedimentation assay (**a**) and quantification of the binding (**b**). $n=3$ independent experiments per group. **c–e**, Subcellular fractionations of *Mark4^{-/-}* or control cardiomyocytes isolated after myocardial infarction. **c**, Representative western blots of the fractions from CEB or PEB derived from the same experiment. **d**, Quantification of the levels of pMAP4(S1046) in CEB, pMAP4(S914) in PEB and VASH2 in PEB ($n=6$ mice per group, blots were processed in parallel). **e**, Correlation between VASH2 level in

the PEB fraction and pMAP4 levels. **f, g**, Stimulated emission depletion images of VASH2 and α -tubulin in *Mark4^{-/-}* or control cardiomyocytes isolated from mice after myocardial infarction. **f**, Representative images. Scale bar, 2 μm. **g**, Pearson correlation coefficient (PCC) of VASH2 and α -tubulin signals, percentage of VASH2 signals on the polymerized microtubules, percentage of VASH2 signals off the polymerized microtubules in the *Mark4^{+/+}* myocardial infarction group ($n=6$ mice, $n=38$ cardiomyocytes examined over 3 independent experiments) and *Mark4^{-/-}* myocardial infarction group ($n=6$ mice, $n=47$ cardiomyocytes examined over 3 independent experiments). **b, d, g**, Data are mean \pm s.e.m. One-way ANOVA (**b**); two-tailed unpaired *t*-test (**d, g**); two-tailed correlation test (**e**). *P* values are indicated.

the polymerized microtubules. Notably, levels of pMAP4(S914) and pMAP4(S1046) were substantially reduced in *Mark4^{-/-}* cardiomyocytes after myocardial infarction (Fig. 4c, d), confirming that S914 and S1046 of MAP4 are substrate sites of the MARK4 kinase. Reduced levels of pMAP4(S1046) in the CEB fraction and pMAP4(S914) in the PEB fraction correlated well with a reduced level of VASH2 in the PEB fraction ($r^2=0.6165, P=0.0025; r^2=0.4529, P=0.0165$, respectively) (Fig. 4c–e), with a stronger association between pMAP4(S1046) and VASH2. In addition, we found that VASH2 levels were positively correlated with desmin levels in the PEB fraction (Extended Data Fig. 8h–j), supporting previous data that detyrosinated microtubules are positively correlated with desmin levels in cardiomyocytes⁵. In summary, our results suggest that MARK4 kinase, through phosphorylation of MAP4 at S914 and S1046, changes the status of MAP4 to allow VASH2 access to the polymerized microtubule for its TCP activity.

To further confirm the causal effect of MARK4 on VASH2 localization, we overexpressed MARK4 in primary cardiomyocytes, which caused the appearance of pMAP4(S1046) (Extended Data Fig. 9a–c) and giant MAP4 puncta in the cytosol (Extended Data Fig. 9d, e) and led to increased VASH2 levels in the PEB fraction (Extended Data Fig. 9a–c). By using stimulated emission depletion super-resolution microscopy³⁴, we found a strong localization of VASH2 on the polymerized microtubules in primary cardiomyocytes isolated from wild-type hearts after myocardial infarction compared with samples isolated from wild-type hearts at baseline (Extended Data Fig. 10a, b). Total VASH2 levels were comparable between *Mark4^{-/-}* and *Mark4^{+/+}* cardiomyocytes after myocardial infarction (Extended Data Fig. 10c, d). However, there was a significant reduction in the association between VASH2 and polymerized microtubules in *Mark4^{-/-}* compared with wild-type cardiomyocytes (Fig. 4f, g). In conclusion, our results demonstrate that MARK4 regulates microtubule detyrosination by phosphorylating MAP4 and controlling VASH2 accessibility to the microtubules (Extended Data Fig. 10e).

Discussion

Detyrosinated microtubules interfere with the contractile function of cardiomyocytes from failing hearts in humans⁷, and targeting the

regulatory mechanism that controls microtubule detyrosination could represent a new inotropic strategy for improving cardiac function. We show that MARK4 has an important role in the alteration of cardiomyocyte contractility through the modulation of microtubule detyrosination in the ischaemic heart. It will be interesting to examine whether this protective effect of MARK4 inactivation on cardiac function after myocardial infarction is sustained in the very long term (several months after myocardial infarction) without inducing any harmful side effects, and whether MARK4 inhibition can improve contractile function in the setting of non-ischaemic heart failure. Furthermore, the marked improvement in relaxation kinetics in the absence of MARK4 raises the possibility of a potential beneficial effect of MARK4 inhibition in the setting of heart failure with preserved ejection fraction, an increasingly common cardiac syndrome that is associated with high morbidity and mortality. The molecular and structural mechanisms of MARK4 coupled with MAP4 and VASH2-SVBP in modifying microtubule detyrosination will need to be investigated in other settings such as mitosis, where regulation of detyrosinated microtubules has important pathophysiological relevance^{9,35}, and the differential role of other TCPs (for example, VASH1) will need to be studied further in future.

Online content

Any methods, additional references, Nature Research reporting summaries, source data, extended data, supplementary information, acknowledgements, peer review information; details of author contributions and competing interests; and statements of data and code availability are available at <https://doi.org/10.1038/s41586-021-03573-5>.

1. Murray, C. J. & Lopez, A. D. Measuring the global burden of disease. *N. Engl. J. Med.* **369**, 448–457 (2013).
2. Packer, M. et al. Effect of oral milrinone on mortality in severe chronic heart failure. *N. Engl. J. Med.* **325**, 1468–1475 (1991).
3. Cohn, J. N. et al. A dose-dependent increase in mortality with vesnarinone among patients with severe heart failure. *N. Engl. J. Med.* **339**, 1810–1816 (1998).
4. Teerlink, J. R. et al. Cardiac myosin activation with omecamtiv mecarbil in systolic heart failure. *N. Engl. J. Med.* **384**, 105–116 (2021).
5. Robison, P. et al. Detyrosinated microtubules buckle and bear load in contracting cardiomyocytes. *Science* **352**, aaf0659 (2016).

6. Anderson, J. L. & Morrow, D. A. Acute myocardial infarction. *N. Engl. J. Med.* **376**, 2053–2064 (2017).
7. Chen, C. Y. et al. Suppression of detyrosinated microtubules improves cardiomyocyte function in human heart failure. *Nat. Med.* **24**, 1225–1233 (2018).
8. Schuldert, M. et al. Proteomic and functional studies reveal detyrosinated tubulin as treatment target in sarcomere mutation-induced hypertrophic cardiomyopathy. *Circ. Heart Fail.* **14**, e007022 (2021).
9. Aillaud, C. et al. Vasohibins/SVBP are tubulin carboxypeptidases (TCPs) that regulate neuron differentiation. *Science* **358**, 1448–1453 (2017).
10. Nieuwenhuis, J. et al. Vasohibins encode tubulin detyrosinating activity. *Science* **358**, 1453–1456 (2017).
11. Chen, C. Y. et al. Depletion of vasohibin 1 speeds contraction and relaxation in failing human cardiomyocytes. *Circ. Res.* **127**, e14–e27 (2020).
12. Wang, N. et al. Structural basis of tubulin detyrosination by the vasohibin–SVBP enzyme complex. *Nat. Struct. Mol. Biol.* **26**, 571–582 (2019).
13. Li, F., Hu, Y., Qi, S., Luo, X. & Yu, H. Structural basis of tubulin detyrosination by vasohibins. *Nat. Struct. Mol. Biol.* **26**, 583–591 (2019).
14. Zhou, C., Yan, L., Zhang, W. H. & Liu, Z. Structural basis of tubulin detyrosination by VASH2/SVBP heterodimer. *Nat. Commun.* **10**, 3212 (2019).
15. Ramkumar, A., Jong, B. Y. & Ori-McKenney, K. M. Remapping the microtubule landscape: how phosphorylation dictates the activities of microtubule-associated proteins. *Dev. Dyn.* **247**, 138–155 (2018).
16. Chinnakkannu, P. et al. Site-specific microtubule-associated protein 4 dephosphorylation causes microtubule network densification in pressure overload cardiac hypertrophy. *J. Biol. Chem.* **285**, 21837–21848 (2010).
17. Doerflinger, H., Benton, R., Shulman, J. M. & St Johnston, D. The role of PAR-1 in regulating the polarised microtubule cytoskeleton in the *Drosophila* follicular epithelium. *Development* **130**, 3965–3975 (2003).
18. Goldstein, B. & Macara, I. G. The PAR proteins: fundamental players in animal cell polarization. *Dev. Cell* **13**, 609–622 (2007).
19. Illenberger, S. et al. Phosphorylation of microtubule-associated proteins MAP2 and MAP4 by the protein kinase p110^{mark}. Phosphorylation sites and regulation of microtubule dynamics. *J. Biol. Chem.* **271**, 10834–10843 (1996).
20. Trinczek, B., Brajenovic, M., Ebneth, A. & Drewes, G. MARK4 is a novel microtubule-associated proteins/microtubule affinity-regulating kinase that binds to the cellular microtubule network and to centrosomes. *J. Biol. Chem.* **279**, 5915–5923 (2004).
21. Drewes, G., Ebneth, A. & Mandelkow, E. M. MAPs, MARKs and microtubule dynamics. *Trends Biochem. Sci.* **23**, 307–311 (1998).
22. Zouggari, Y. et al. B lymphocytes trigger monocyte mobilization and impair heart function after acute myocardial infarction. *Nat. Med.* **19**, 1273–1280 (2013).
23. Pell, V. R. et al. Ischemic preconditioning protects against cardiac ischemia reperfusion injury without affecting succinate accumulation or oxidation. *J. Mol. Cell. Cardiol.* **123**, 88–91 (2018).
24. Li, X. et al. MARK4 regulates NLRP3 positioning and inflammasome activation through a microtubule-dependent mechanism. *Nat. Commun.* **8**, 15986 (2017).
25. Clement, M. et al. MARK4 (microtubule affinity-regulating kinase 4)-dependent inflammasome activation promotes atherosclerosis—brief report. *Arterioscler. Thromb. Vasc. Biol.* **39**, 1645–1651 (2019).
26. Toldo, S. & Abbate, A. The NLRP3 inflammasome in acute myocardial infarction. *Nat. Rev. Cardiol.* **15**, 203–214 (2018).
27. Baldrihi, M., Mallat, Z. & Li, X. NLRP3 inflammasome pathways in atherosclerosis. *Atherosclerosis* **267**, 127–138 (2017).
28. Ackers-Johnson, M. et al. A simplified, Langendorff-free method for concomitant isolation of viable cardiac myocytes and nonmyocytes from the adult mouse heart. *Circ. Res.* **119**, 909–920 (2016).
29. Kuhns, S. et al. The microtubule affinity regulating kinase MARK4 promotes axoneme extension during early ciliogenesis. *J. Cell Biol.* **200**, 505–522 (2013).
30. Szyk, A., Deaconescu, A. M., Piszczeck, G. & Roll-Mecak, A. Tubulin tyrosine ligase structure reveals adaptation of an ancient fold to bind and modify tubulin. *Nat. Struct. Mol. Biol.* **18**, 1250–1258 (2011).
31. Arce, C. A. & Barra, H. S. Release of C-terminal tyrosine from tubulin and microtubules at steady state. *Biochem. J.* **226**, 311–317 (1985).
32. Kellogg, E. H. et al. Near-atomic model of microtubule–tau interactions. *Science* **360**, 1242–1246 (2018).
33. Shigematsu, H. et al. Structural insight into microtubule stabilization and kinesin inhibition by tau family MAPs. *J. Cell Biol.* **217**, 4155–4163 (2018).
34. Bottanelli, F. et al. Two-colour live-cell nanoscale imaging of intracellular targets. *Nat. Commun.* **7**, 10778 (2016).
35. Barisic, M. et al. Microtubule detyrosination guides chromosomes during mitosis. *Science* **348**, 799–803 (2015).

Publisher's note Springer Nature remains neutral with regard to jurisdictional claims in published maps and institutional affiliations.

© The Author(s), under exclusive licence to Springer Nature Limited 2021

Article

Methods

Data reporting

The experiments were randomized when possible, and the investigators were blinded to allocation during experiments and outcome assessment when possible (further information on randomization and blinding is available in the Nature Research Reporting Summary linked to this Article).

Mice

All in vivo experiments using mice were approved by the UK Home Office and were performed under PPL PA4BDF775. All mice were on a C57BL/6 background and housed under standard temperature (18–23 °C) and humidity (40–60%), with a 12-h light–dark cycle. *Mark4^{-/-}* mice were provided by Y. Shi²⁴ and Mutant Mouse Resource and Research Center; *Myh6-mcm^{+/+}* Cre mice were originally from the Jackson Laboratory (Cre was expressed under mouse cardiac-specific α-myosin heavy chain promoter (α-MHC; Myh6)); *Mark4^{fl/fl}* mice were from Taconic Biosciences. *Myh6-mcm^{+/+}* Cre mice were crossed with *Mark4^{fl/fl}* mice to generate *Myh6-mcm^{+/+/-}cre;Mark4^{fl/fl}* mice. The Cre-mediated excision of floxed *Mark4* alleles was induced by treatment with tamoxifen dissolved in corn oil by intraperitoneal injection at 20 mg kg⁻¹ body weight per day for 5 consecutive days.

Left anterior descending coronary artery ligation model

Permanent left anterior descending (LAD) coronary artery ligation was performed on mice as previously described^{22,23} with minor modifications. Mice, at 8–10 weeks of age, were anaesthetized using ketamine at 100 mg kg⁻¹ body weight and xylazine at 10 mg kg⁻¹ body weight by intraperitoneal injection, and then intubated and ventilated with air (supplemented with oxygen) using a small-animal respirator. A thoracotomy was performed in the fourth left intercostal space. The left ventricle was visualized and the pericardial sac was ruptured to expose the LAD coronary artery. The LAD was permanently ligated using a 7-0 Prolene suture. The suture was passed approximately 2 mm below the tip of the left auricle. Marked colour changes of the ischaemic area and ECG changes were monitored as an indication of successful coronary artery occlusion. The thoracotomy was closed with 6-0 Prolene sutures. Sham-operated mice underwent the same procedure without coronary artery ligation. The endotracheal tube was removed once spontaneous respiration resumed, and the mice were placed in a warm recovery cage maintained at 37 °C until they were completely awake. At the indicated time points in the experimental timeline, the mice were euthanized by CO₂ asphyxiation and the tissues were subsequently collected for analysis.

Bone marrow transplants

Eight-to-ten-week-old C57BL/6 mice were maintained overnight with Baytril (Bayer) before irradiation with two doses of 5.5 Gy (separated by 4 h) followed by reconstitution with 1 × 10⁷ sex-matched donor bone marrow cells. Mice were randomly assigned to receive the *Mark4^{-/-}* or *Mark4^{+/+}* bone marrow. Mice were then maintained on Baytril for a 4-week recovery period before performing LAD ligation.

Echocardiography

Transthoracic echocardiography was performed on all mice using Vevo 3100 with a MX400 linear array transducer (VisualSonics), 30 MHz. Mice were anaesthetized with 2–3% isoflurane and kept warm on a heated platform (37 °C). The chest hairs were removed using depilatory cream and a layer of acoustic coupling gel was applied to the thorax. After alignment in the transverse B-mode with the papillary muscles, cardiac function was measured on M-mode images. Echocardiography data were collected using VisualSonics Vevo 3100 and analysed using Vevo LAB3.1.1.

Histological analysis

Whole hearts were excised at different time point after LAD ligation, rinsed in PBS and fixed with 4% PFA overnight at 4 °C. Fixed tissues were thoroughly washed in PBS, and then immersed in 30% sucrose. Tissues were embedded and sectioned by a cryostat into 10-μm thick slices, which started at the apex and ended at the suture ligation site. Masson's trichrome staining was performed to determine scar size. Scar size was calculated as the total infarct circumference divided by the total left ventricle circumference. Some hearts were excised at 24 h after myocardial infarction and quickly sliced into four 1.0-mm thick sections perpendicular to the long axis of the heart. The sections were then incubated with 1% triphenyltetrazolium chloride (TTC, Sigma) for 15 min at 37 °C and digitally photographed. To analyse the infarct size at 24 h after myocardial infarction, the TTC-stained area and TTC-negative area (infarcted myocardium) were measured using ImageJ (v.2.0). Myocardial infarct size was expressed as a percentage of the total left ventricle area. Images were obtained using a Leica DM6000 B microscope, collected using LAS AF software (2.4.0 build 6254) and analysed using ImageJ (v.2.0).

Tissue immunohistochemistry

Whole hearts were excised, quickly washed in PBS and flash-frozen. Tissues were then embedded and cryo-sectioned. Slices were fixed in pre-chilled methanol for 10 min at -20 °C. After washing with PBST (0.1% Tween-20 in 1× PBS), slices were incubated with 3% H₂O₂ (in PBS) for 10 min, and then with blocking buffer (5% BSA in PBST) for 1 h at room temperature. The primary antibody against MARK4 (Abcam, ab124267, used at 1:200) or rabbit IgG isotype control (Novus Biologicals, NB810-56910, used at 1:1,000) was used overnight at 4 °C. Extensive washing steps were performed to remove nonspecific antibody binding. Slices were incubated with the biotinylated secondary antibody (Abcam, ab6720, used at 1:800) for 1 h at room temperature. Reagents A and B from the Avidin-Biotin Complex kit (VECTOR, PK-4000) were diluted and added to the slides. The slides were stained with ImmPACT DAB peroxidase substrate (VECTOR, SK-4105) and counterstained with haematoxylin. Images were obtained using a Leica DM6000 B microscope, collected using LAS AF software (2.4.0 build 6254) and analysed using ImageJ (v.2.0) analyse tools.

Microtubule co-sedimentation assay

Lyophilized porcine brain tubulin (T240) was purchased from Cytoskeleton. Recombinant proteins of 4R-MAP4 and VASH2-SVBP were previously described^{12,33}. Desiccated tubulin was reconstituted in the microtubule polymerization buffer to 10 mg ml⁻¹. To generate polymerized microtubules, tubulin was diluted to 2 mg ml⁻¹ in the polymerization buffer (80 mM K-PIPES, pH 6.8, 1 mM MgCl₂, 1 mM EGTA and 1 mM DTT), supplemented with 5% glycerol and 1 mM GTP at 37 °C for 30 min, and then stabilized by incubating with 2.5 μM taxol at 37 °C for 15 min. The taxol-stabilized microtubules were centrifuged over a cushion buffer (polymerization buffer with 40% glycerol) at 131,700g at 37 °C for 15 min to remove the free tubulin. The pellet was resuspended in the polymerization buffer with 1 μM taxol. Taxol influenced the association of 4R-MAP4 with the microtubules in our assay. 4R-MAP4 association was facilitated when taxol was completely excluded from the buffer. The microtubules without taxol were susceptible to depolymerization if stored at room temperature. In these conditions, the polymerized microtubules were maintained at 37 °C throughout the experiment. For the co-sedimentation assay, the microtubules were mixed with various concentrations of 4R-MAP4 (1–6 μM) and VASH2-SVBP (1–4 μM) in the polymerization buffer. In the competition experiments, the microtubules were incubated with specified 4R-MAP4 concentrations (1–4 μM) for 10 min, followed by addition of a constant amount of VASH2-SVBP (3 μM) with further incubation for 10 min. Subsequently, the reaction mixture was centrifuged using a TLA120.2 rotor at 55,000 rpm for

15 min. The pellet fraction containing the microtubules and bound proteins was resuspended in the loading buffer. The samples were loaded on a 10% SDS-PAGE gel and stained with colloidal Coomassie blue dye (ThermoFisher). The experiments were repeated at least three times. The band intensities were analysed using ImageJ (v.2.0).

Mouse cardiomyocyte isolation

Preparation of cardiomyocytes was accomplished as previously described²⁸. In brief, mice were anaesthetized and the chest was opened to expose the heart. the descending aorta was cut and the heart was immediately flushed by injection of 7 ml EDTA buffer into the right ventricle. The ascending aorta was clamped and the heart was transferred to a 60-mm dish containing fresh EDTA buffer. Digestion was achieved by sequential injection of 10 ml EDTA buffer (NaCl, 130 mM; KCl, 5 mM; NaH₂PO₄, 0.5 mM; HEPES, 10 mM; glucose, 10 mM; BDM, 10 mM; taurine, 10 mM; EDTA, 5 mM; pH to 7.8), 3 ml perfusion buffer (NaCl, 130 mM; KCl, 5 mM; NaH₂PO₄, 0.5 mM; HEPES, 10 mM; glucose, 10 mM; BDM, 10 mM; taurine, 10 mM; MgCl₂, 1 mM; pH to 7.8) and 30–50 ml collagenase buffer (collagenase 2, 0.5 mg ml⁻¹; collagenase 4, 0.5 g ml⁻¹; protease XIV, 0.05 mg ml⁻¹; made fresh and diluted in perfusion buffer) into the left ventricle. The left ventricle was then separated and gently pulled into 1-mm pieces using forceps. Cellular dissociation was completed by gentle trituration, and enzyme activity was inhibited by addition of 5 ml stop buffer (perfusion buffer containing 5% sterile FBS). The cell suspension was passed through a 100-μm filter. Cells underwent four sequential rounds of gravity settling, using three intermediate calcium reintroduction buffers (buffer 1, 75% perfusion buffer with 25% culture medium; buffer 2, 50% perfusion buffer with 50% culture medium; buffer 3, 25% perfusion buffer with 75% culture medium; culture medium comprised 0.1% BSA, 1% ITS, 10 mM BDM, 1% CD lipid and 5% penicillin–streptomycin in M199) to gradually restore the calcium concentration to physiological levels.

Primary cardiomyocyte culture and adenoviral transduction

Adenoviral vectors including pAdeno-SV40-GFP-Blank vector (Adv-null), pAdeno-Ttl-SV40-GFP vector (Adv-Ttl) (NM_027192.2) and pAdeno-Mark4-SV40-GFP vector (Adv-Mark4) (NM_172279.1) were purchased from Applied Biological Materials. Adenoviral vector pAV[shRNA]-EGFP-U6>mMap4 (*Map4* shRNA target sequence: AGAGTG-GACTATCCGGATTAT), adenoviral vector pAV[shRNA]-EGFP-U6>mVash2 (*Vash2* shRNA target sequence: GAGAACCTGCTTCTAAAT) and adenoviral vector pAV[shRNA]-EGFP-U6>Scramble were purchased from VectorBuilder. Six-well plates or coverslips were coated with laminin at a final concentration of 5 μg ml⁻¹ in PBS overnight at 4 °C. The wells were washed and air-dried for 10 min before plating cells. After collecting the cells by gravity settling and calcium re-introduction, the final cardiomyocyte pellets were resuspended in 2 ml culture medium and 2 ml pre-equilibrated plating medium (0.1% FBS, 10 mM BDM and 5% penicillin–streptomycin in M199) for culture. After incubation for 1 h, the cell medium was changed with pre-equilibrated culture medium and adenovirus vectors were administered at 5 × 10⁶ PFU ml⁻¹. After co-culture with virus for 8 h, fresh culture medium was used to wash and replace the old culture medium containing the virus. Cells were either used for the contractility assay and western blotting immediately after the medium change (in the experiments of overexpression of TTL), or collected at 48 h after transduction (in the experiments of *Mark4* over-expression, *Map4* shRNA and *Vash2* shRNA) for the subsequent assays.

Cardiomyocyte contractility assay

Sarcomere shortening and relaxation were measured in freshly isolated left ventricular cardiomyocytes of mouse hearts using the integrated IonOptix contractility/photometry system. Cardiomyocytes were maintained in normal Tyrode's solution (NaCl, 140 mM; MgCl₂, 0.5 mM; NaH₂PO₄, 0.33 mM; HEPES, 5 mM; glucose, 5.5 mM; CaCl₂, 1 mM; KCl, 5 mM; NaOH, pH to 7.4) at room temperature, electrically stimulated

at 2 Hz using a field stimulator, and changes in sarcomere length were recorded. Basal and peak sarcomere length, maximum departure and return velocities and time to peak were measured. All measurements were performed at room temperature. For parthenolide (PTL) experiments, cardiomyocytes were treated with 10 μM PTL (Sigma P0667) or vehicle at room temperature in normal Tyrode's solution for 1 h before contractility measurements, and the vehicle–dimethyl sulfoxide (DMSO)–diluted in the same way was applied as control. All measurements were performed at room temperature within 4 h. Data were collected and analysed using IonWizard 7.4.

Calcium measurements

Measurement of intracellular calcium was performed in freshly isolated left ventricular cardiomyocytes using the integrated IonOptix contractility/photometry system. Cardiomyocytes were loaded with 1 μM Fura-2-AM for 20 min (protected from light) and then washed to allow de-esterification for 20 min. Cells were then rinsed with normal Tyrode's solution. Cells were stimulated at 2 Hz using a field stimulator with dual excitation (at 360 and 380 nm), and emission light was collected at 510 nm. Changes in calcium transients were recorded using IonOptix software. All of the cells analysed were beating. All measurements were performed at room temperature within 4 h. Data were collected and analysed using IonWizard 7.4.

Immunofluorescence and image acquisition

Cardiomyocytes were fixed with pre-chilled methanol for 10 min, then washed twice using PBST (0.1% Tween-20 in 1× PBS) with 5-min intervals. Cells were blocked for 1 h at room temperature with blocking buffer (5% BSA in PBST) and incubated with primary antibodies overnight at 4 °C. The primary antibodies were: detyrosinated α-tubulin (Abcam, ab48389, used at 1:200), α-tubulin (CST, 3873S, used at 1:200), MARK4 (Abcam, ab124267, used at 1:200), APC anti-mouse CD45 (BioLegend, 103112, used at 1:200) and rabbit IgG isotype control (Novus Biologicals, NB810-56910, used at 1:2,000). The cells were then washed with PBST and incubated with secondary antibody for 1 h at room temperature. The secondary antibodies were: AF488 donkey anti-rabbit IgG (Invitrogen, A21206, used at 1:200), AF647 goat anti-mouse IgG (Invitrogen, A21236, used at 1:200), AF647 goat anti-rat IgG (Invitrogen, A21247, used at 1:200). DAPI (Sigma, 10236276001, used at 1:1,000) was used. Confocal images were obtained using a Leica SP5 confocal laser scanning microscope, collected using LAS AF software (2.7.3.9723) and analysed using ImageJ (v.2.0) analyse tools.

Stimulated emission depletion imaging and image analysis

Cardiomyocytes on coverslips were fixed with 100% methanol for 15 min at room temperature and then washed three times with PBS (5-min intervals). Cells were blocked with buffer (5% BSA and 0.2% Triton X-100 in PBS) for 30 min, then incubated with primary antibodies (diluted in blocking buffer) overnight at 4 °C. The primary antibodies were VASH2 (Abcam, ab224723, used at 1:200), MAP4 (Abcam, ab245578, used at 1:200) and α-tubulin (CST, 3873S, used at 1:200). The cells were washed three times using wash buffer (0.05% Triton X-100 in PBS) at room temperature, then incubated with the secondary antibody for 1 h at room temperature. The secondary antibodies were: Atto-594 goat anti-rabbit IgG (Sigma, 77671, used at 1:500) and Atto-647N goat anti-mouse IgG (Sigma, 50185, used at 1:500). Cells were then washed three times in wash buffer. Cells were fixed (3% paraformaldehyde and 0.1% glutaraldehyde diluted in PBS) followed by three washes in PBS. The coverslips were then mounted on the slide.

Stimulated emission depletion (STED) imaging was carried out on a custom multicolour system with three pulsed excitation lines, one fixed depletion line, fast 16 kHz beam scanning and gated detection centred around an Olympus IX83 microscope base. This system uses identical hardware, and a closely matched optical arrangement, to a previously described system³⁴. In brief, two-colour STED imaging was performed

Article

sequentially. Images were acquired with a $100\times$ oil-immersion objective lens (Olympus, UPLSAPO 100XO/PSF). Fields of view between 23 and 27 μm^2 were imaged with a $1,024 \times 1,024$ image format and an approximately 20 nm pixel size. Excitation powers were between 15 and 30 μW at the microscope side port and the STED depletion power was approximately 120 mW at the microscope side port. Fast, 16 kHz, unidirectional beam scanning with blanking was used to minimize light exposure. Each line of an image was scanned 850 times, resulting in an image acquisition time of approximately 54 s per colour. STED image data were collected with a custom program written in National Instrument (NI) LabVIEW 2014 64-bit, NI FPGA Module and NI Vision Development Module.

MAP4 oligomerized puncta (with a diameter longer than 400 nm) were measured and calculated using ImageJ (v.2.0). The number of puncta was normalized against the cell area of each image.

For the acquired images, a dynamic thresholding algorithm was used for the image analysis. Images were converted into HSV colour images (C) with information of hue (h), saturation (s) and value (v). $C(i,j)$ was assumed as a non-background image pixel, N was the total number of non-background image pixels, H was image height and W was image width. The average of all the non-background image pixels was calculated as $k = (\sum_{i=1}^H \sum_{j=1}^W C(i,j))/N$. The following three thresholds were applied to discriminate signals: $h = [0, 180]$; $s = [0, 43]$; $v = [k + 30, 220]$. A Gaussian filter $f(x) = \frac{1}{2\pi\sigma^2} e^{-\frac{x^2+y^2}{2\sigma^2}}$, a two-dimensional convolution operator, was used to remove noise. For the VASH2 signals, the Gaussian filter with a kernel of 3×3 was used for image denoising. For the linear microtubule signals, the Gaussian filter with a kernel of 5×5 was used for image denoising when $k \geq 35$ and a kernel of 3×3 was applied when $k < 35$. The total numbers of VASH2 (v) and α -tubulin (t) pixels were calculated. The total number of overlapping image pixels (o) between VASH2 and tubulin was calculated as VASH2 signals on the microtubules, and $(1 - o)/v$ was calculated as VASH2 signals off the microtubules. The Pearson correlation coefficient ($\rho_{x,y} = \frac{\text{cov}(X,Y)}{\sigma_x \sigma_y}$) between VASH2 signals and tubulin signals was calculated. Automatic image processing was coded using a custom algorithm in Python v.3.7.8.

Subcellular fractionations of the primary cardiomyocytes

Subcellular fractionations of primary cardiomyocytes were performed according to the manufacturer's instructions (Pierce, 87790). In brief, cells were incubated with CEB, which selectively permeabilizes the cell membrane for 10 min at 4 °C with gentle mixing. Cells were centrifuged for 5 min at 500g and supernatants were collected. The cytoskeletal binding proteins were isolated in the PEB.

Subcellular fractionations of primary cardiomyocytes were also obtained using a conventional method. Primary mouse cardiomyocytes were isolated and homogenized in pre-warmed (37 °C) microtubule-stabilizing buffer (PIPES, 80 mM; MgCl₂, 1 mM; EGTA, 1 mM; 0.5% Triton X-100; 10% glycerol; GTP, 0.5 mM; Halt protease inhibitor cocktail from Thermo Fisher Scientific 1862209; pH to 6.8) using a Dounce homogenizer. The homogenates were centrifuged at 100,000g for 15 min at room temperature. The supernatants were collected as the free-tubulin fraction as F1, and the pellets were dissolved in the microtubule-destabilizing buffer (Tris-HCl, 20 mM; NaCl, 150 mM; 1% Triton X-100; CaCl₂, 10 mM; Halt protease inhibitor cocktail from Thermo Fisher Scientific 1862209; pH to 7.4) for further incubation on ice for 1 h to depolymerize the microtubules. The dissolved lysates were centrifuged at 12,000g for 15 min at 4 °C. The pellets were incubated with 150 units of micrococcal nuclease (100 units μl^{-1} , Thermo Fisher Scientific, 88216) in microtubule-destabilizing buffer for 15 min at room temperature, and then centrifuged at 12,000g for 5 min at 4 °C to remove the nuclear debris. The collected pellets were dissolved in 2× SDS

buffer (4% SDS; 20% glycerol; Tris-HCl, 0.25 M; pH to 6.5). The dissolved lysates were then centrifuged at 14,000g for 5 min at 4 °C. The supernatants were collected as F2 (extraction from the stable pellet fraction) and the residual pellets were kept.

Western blotting

The heart tissues were grounded thoroughly with a mortar and pestle in liquid nitrogen. Tissue powder was lysed using Triton lysis buffer (20 mM Tris-HCl, pH to 7.5; 150 mM NaCl; 1 mM Na₂EDTA; 1 mM EGTA; 1% Triton X-100; 1 mM Na₃VO₄; 5 mM NaF; protease inhibitor cocktail (ThermoFisher, 1862209)). The supernatant (soluble fraction) was collected, and the pellets (insoluble fraction) were dissolved in 8 M urea (Figs. 1b, 3a, d; $n = 12$ mice in the *Mark4*^{+/+} myocardial infarction group and $n = 9$ mice in the *Mark4*^{-/-} myocardial infarction group used for Fig. 3b). For some experiments ($n = 8$ mice per group used for Fig. 3b, c), heart tissues were homogenized in the lysis buffer (0.1 M PIPES pH to 6.8; 2 mM EGTA; 0.1 mM EDTA; 0.5 mM MgCl₂; 20% glycerol; 0.1% Triton X-100; protease inhibitor cocktail (ThermoFisher, 1862209)) and incubated for 30 min at 37 °C. After centrifugation (21,100g for 5 min), the supernatants were collected as the soluble fraction, and the pellets were dissolved in buffer (RIPA buffer (CST, 9806); 0.8% SDS; and protease inhibitor cocktail (ThermoFisher, 1862209)) and collected as the insoluble fraction. The protein concentration was determined using a BCA protein assay kit (ThermoFisher, 23235). Molecular mass markers (ThermoFisher, LCS603 and LC5925) were used. Supernatant samples were prepared in NuPAGE LDS sample buffer (Invitrogen) and run on NuPAGE 4–12% Bis-Tris gels (Invitrogen). Pellet samples were prepared in Tris-glycine SDS sample buffer (Invitrogen) and run on Novex 4–20% Tris-glycine gels (Invitrogen). All samples were blotted onto a PVDF membrane after electrophoresis. The following primary antibodies were used in the experiments: MARK4 (CST, 4834S, used at 1:1,000), GAPDH (CST, 5174S, used at 1:1,000), desmin (R&D, AF3844, used at 1:1,000), detyrosinated α -tubulin (Abcam, ab48389, used at 1:200), polyglutamylated α -tubulin (AdipoGen, AG-20B-0020-C100, used at 1:1,000), acetylated α -tubulin (Santa Cruz Biotechnology, sc23950, used at 1:1,000), α -tubulin (CST, 3873S, used at 1:200). After antibody detection, membranes were revealed with ECL. Quantification of the western blot bands was performed using ImageJ (v.2.0).

For the fractionation assay, equal amounts of total protein (20 μg) from each fraction were used for western blot. The DC protein assay kit (Bio-Rad, 5000111) was used to measure protein concentrations. Across different gels, equal amounts of a molecular mass marker (ThermoFisher, LCS603) were loaded in each gel. Samples were run on NuPAGE 4–12% Bis-Tris gels (Invitrogen) and blotted onto a PVDF membrane.

Some samples of the CEB fraction from the fractionation assay were prepared for native gel analysis. Samples were processed in Tris-glycine native sample buffer (ThermoFisher, LC2673) before loading without heating or addition of any reducing reagent. Samples were loaded on a 3–8% NuPAGE Tris-acetate gel (ThermoFisher, EA0375BOX) for electrophoresis in Tris-glycine native running buffer (Tris-base, 25 mM; glycine, 192 mM; pH to 8.3). Native molecular marker (ThermoFisher, LC0725) was used. After electrophoresis, proteins were transferred to a PVDF membrane by transfer buffer (Bicine, 25 mM; Bis-Tris, 25 mM; EDTA, 1 mM; pH to 7.2).

Some samples from the fractionation assay were prepared with a denaturing treatment by adding urea. Urea (0 M, 2 M, 4 M or 8 M) was added to the samples as indicated. A micro-BCA protein assay kit (ThermoFisher, 23235) was used to measure protein concentrations if urea was added to the samples. Samples were then processed in Tris-glycine SDS sample buffer (ThermoFisher, LC2676) and reducing reagent (10% 2-mercaptoethanol). A 4–20% Tris-glycine gel (ThermoFisher, EC6026BOX) was used for electrophoresis in Tris-glycine SDS running buffer (Tris-base, 25 mM; glycine, 192 mM; 0.1% SDS; pH to 8.3).

After electrophoresis, proteins were transferred to PVDF membrane by transfer buffer (Tris-base, 12 mM; glycine, 96 mM; pH to 8.3).

The primary antibodies used for fractionation assays were: detyrosinated α -tubulin (Abcam, ab48389, used at 1:1,000), α -tubulin (CST, 3873S, used at 1:1,000), TTL (Proteintech, 13618-1-AP, used at 1:1,000), VASH1 (Abcam, ab199732, used at 1:1,000), VASH2 (Abcam, ab224723, used at 1:1,000), pMAP4(S1073) (Abnova, PAB15916, used at 1:1,000), MAP4 (Abcam, ab245578, used at 1:1,000), pMAP4(S941) (Abcam, ab56087, used at 1:1,000), GAPDH (CST, 5174S, used at 1:1,000), desmin (R&D, AF3844, used at 1:1,000). Membranes were revealed with ECL. Quantification of western blot bands was performed using ImageJ (v.2.0). The band density was normalized in two steps: (1) the density of the targeted band was first normalized against the density of the loading molecular mass marker band (norm 1); (2) the value of norm 1 was internally normalized against the average value of norm 1 of the control group (norm 2). The finalized value (norm 2) was used to compare the fold changes against the value of the control groups across different gels. desmin was used as a marker for the pellet fraction, and GAPDH was used as a marker for the cytosolic fraction. Coomassie-blue-stained gels loaded with the same amounts of proteins as used in western blotting experiments or Ponceau-S-stained membranes after the transfer step were used to confirm equal loading. All of the immunoblots, gels and membranes associated with the data presented in the figures and extended data figures are provided (Supplementary Fig. 1).

Heart tissue digestion and flow cytometry

Hearts were collected and the left ventricle was isolated, minced with fine scissors and subjected to enzymatic digestion solution (RPMI 1640, collagenase D (0.2 mg ml⁻¹, Roche), dispase (1 U ml⁻¹, StemCell Technologies) and DNase I (0.2 mg ml⁻¹, Sigma)) for 45 min at 37 °C. Cells were collected, filtered through a 40- μ m nylon mesh and washed with PBS with 2.5% v/v fetal bovine serum. Cell suspensions were incubated with a Zombie Aqua Fixable Viability Kit (Biolegend, 423102, used at 1:1,000) for 20 min at room temperature and washed with PBS. Cells were then stained with fluorescently labelled anti-mouse antibodies, including APC anti-mouse CD45 (Biolegend, 103112, used at 1:100), AF488 anti-mouse CD11b (Biolegend, 101217, used at 1:100), Pacific blue anti-mouse Ly6G (Biolegend, 127612, used at 1:100), PE anti-mouse F4/80 (Biolegend, 123110, used at 1:100), PECY7 anti-mouse CD11c (Biolegend, 117318, used at 1:100), Brilliant Violet 605 anti-mouse CD3 (Biolegend, 100237, used at 1:100) and FITC anti-mouse CD19 (Biolegend, 553785, used at 1:100), diluted in staining buffer for 30 min at 4 °C in the presence of 24G2Fc receptor blocker (obtained from the Division of Immunology, Department of Pathology, University of Cambridge), before extensive washing. The cytometric acquisition was performed on a LSR II Fortessa (BD biosciences). Cell analysis was done using BD FACSDiva Software 6.0 and FlowJo software (v.10).

Real-time PCR

For gene expression analysis, RNA from heart tissues or separated cardiomyocytes was isolated using an RNAeasy mini kit (Qiagen). Reverse transcription was performed using a QuantiTect reverse-transcription kit (Qiagen). qRT-PCR was performed with SYBR Green qPCR mix (Eurogentec) using the Roche LightCycler 480II. Primer sequences are as follows: *Mark4* (forward 5'-GGACACCGATGGCACATTG-3'; reverse 5'-GCAGGAAGCGATAGAGTTCCG-3'); *Vash2* (forward 5'-GCC TTCCTGGCTAACGCCTTC-3'; reverse 5'-CCCTGTGGTTGTATTGT AGAG-3'); *Hprt* (forward 5'-TCACTAACGGGGACATAAA-3'; reverse 5'-GGGGCTGTACTGCTTAACCAG-3'); *Rpl4* (forward 5'-CCGT CCCCTCATATCGGTGTA-3'; reverse 5'-GCATAGGGCTGCTGTGTT GTTTTT-3'); *Rpl13a* (forward 5'-AGCCTACCAAGAAAGTTGCTTAC-3'; reverse 5'-GCCTCTTCTCCGATACTGCATC-3'). The average of three housekeeping genes (*Hprt*, *Rpl4* and *Rpl13a*) was used as reference for qPCR gene expression analysis.

Measurement of cardiac troponin I and inflammatory cytokines

Serum was collected within 24 h after myocardial infarction or at day 3 after myocardial infarction. Measurements of the cardiac injury biomarker (collected within 24 h) and cytokines (collected at day 3 after myocardial infarction) were performed by the core biochemical assay laboratory of Cambridge University Hospitals.

Statistics and reproducibility

All values in the text and figures are presented as mean \pm s.e.m. of independent experiments with given *n* sizes. No statistical methods were used to predetermine sample size. Statistical analysis was performed with Prism v.7.05 (GraphPad) and Excel (Microsoft Excel 2102). Violin plots were created with Prism v.9.1.0 (216) (GraphPad). Data were tested for normality using a Kolmogorov-Smirnov test. Group comparisons were analysed using two-tailed analyses. Comparisons of three or more groups were analysed using one-way (one variable) or two-way (two variables) ANOVA followed by the Bonferroni post hoc correction for multiple comparisons when appropriate. *P*<0.05 was considered statistically significant.

Data in Figs. 1b, c, 3a and Extended Data Figs. 2a, 5a, 7b, 8a, b are representative of three independent experiments. Data in Extended Data Fig. 8e-g are representative of two independent experiments.

Reporting summary

Further information on research design is available in the Nature Research Reporting Summary linked to this paper.

Data availability

All of the associated raw data presented in this paper are available from the corresponding author upon request. Source data are provided with this paper.

Code availability

Custom STED microscope control software used for data collection can be accessed at <https://github.com/Gurdon-Super-Res-Lab/STED-Control>, and a customized algorithm used for STED image analysis is available at https://github.com/zhaoaite/dynamic_thresholding_algorithm.

Acknowledgements The work is supported by a British Heart Foundation (BHF) fellowship grant (FS/14/28/30713) to X.L., an Isaac Newton Trust grant (18400) to X.L. and Cambridge BHF Centre of Research Excellence grants (RE/13/6/30180 and RE/18/1/34212) to X.L. X.Y. was supported by a Royal Society Newton Advanced Fellowship grant (NA140277) and is supported by BHF grants (FS/14/28/30713, RE/18/1/34212). Z.M. is supported by BHF chair grant (CH/10/001/27642) and the NIHR Cambridge Biomedical Research Centre. M.A.-N. is supported by German Research Foundation (Deutsche Forschungsgemeinschaft (DFG)) (AM 507/1). G.S., E.A. and D.S.J. are supported by a Wellcome Trust collaborative award (203285), a Wellcome Principal Research Fellowship (207496) and core support from the Wellcome Trust (203144) and Cancer Research UK (A24823). The work of H.Z. is supported in part by a Royal Society Newton Advanced Fellowship grant (NA160342). We thank staff at the phenotyping hub and biochemical assay laboratory of Cambridge University Hospitals; staff at the Phenomics Laboratory and Anne McLaren Building of Cambridge University; B. Prosser for sharing protocols and discussion; M. Zhang for advice on echography data; M. A. Ackers-Johnson from R. Foo's laboratory for technical advice on isolating and culturing primary mouse cardiomyocytes; S. Ozanne and L. Pantaleo for access and training of ultracentrifuge use; D. Pavlovic for advice on IonOptix; C. Huang for advice on calcium measurements; T. Zhao for his intellectual discussion and reading the manuscript; and X. Luo, who passed away due to COVID-19 during the outbreak in Wuhan, for her support of this project.

Author contributions X.Y., X.C., M.A.-N., A.Z., H.Z. and X.L. designed the experiments. X.Y., X.C., M.A.-N., E.A., A.Z., H.C., M.C., J.H. and X.L. performed the experiments. X.Y., X.C., M.A.-N., H.C., A.Z., H.Z. and X.L. analysed the data. X.Y. performed all of the *in vivo* experiments using mouse models and contractility assays, and wrote the relevant Methods section. X.C. performed the primary cardiomyocyte isolation, fractionation, real-time PCR, western blotting and imaging experiments. M.A.-N. performed *in vitro* microtubule co-sedimentation assay, analysed the data and wrote the relevant Methods section. E.A. configured the custom STED system, performed STED imaging and wrote the relevant Methods section. G.S. provided assistance for STED imaging. A.Z. and H.Z. wrote the STED image analytic code, analysed STED data and wrote the

Article

relevant Methods section. H.C. assisted with tissue collection, performed tissue sectioning and staining assays, and optimized some of the experimental conditions. M.C. assisted with part of the tissue collection, staining and analysis. J.H. provided some technical supports on mouse experiments. C.D., H.C. and X.L. performed the initial test. H.H. and K.T. provided recombinant proteins. T.K. provided initial training for the LAD model. D.S.J. provided the super-resolution imaging platform. Z.M. independently had the idea and supported the initiation of the project (the mouse *in vivo* work was performed under the Procedure Project Licence of Z.M.). X.Y., X.C., Z.M. and X.L. interpreted the data for important intellectual contents. X.L. conceived idea, designed and initiated the project, established the collaboration, supervised the project, and wrote the manuscript. All authors reviewed and edited the manuscript.

Competing interests The authors declare no competing interests.

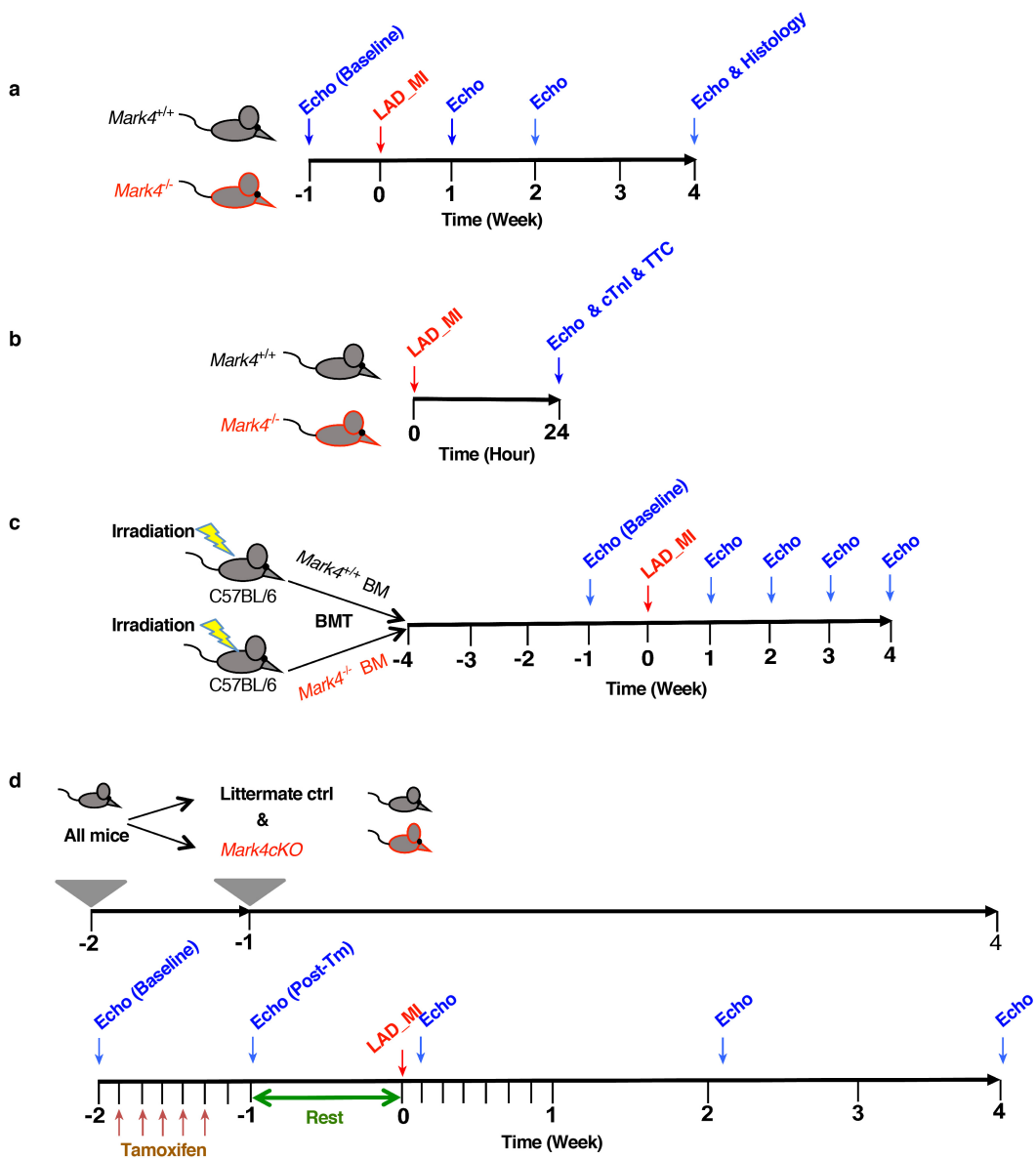
Additional information

Supplementary information The online version contains supplementary material available at <https://doi.org/10.1038/s41586-021-03573-5>.

Correspondence and requests for materials should be addressed to X.L.

Peer review information *Nature* thanks Leslie Leinwand and the other, anonymous, reviewer(s) for their contribution to the peer review of this work.

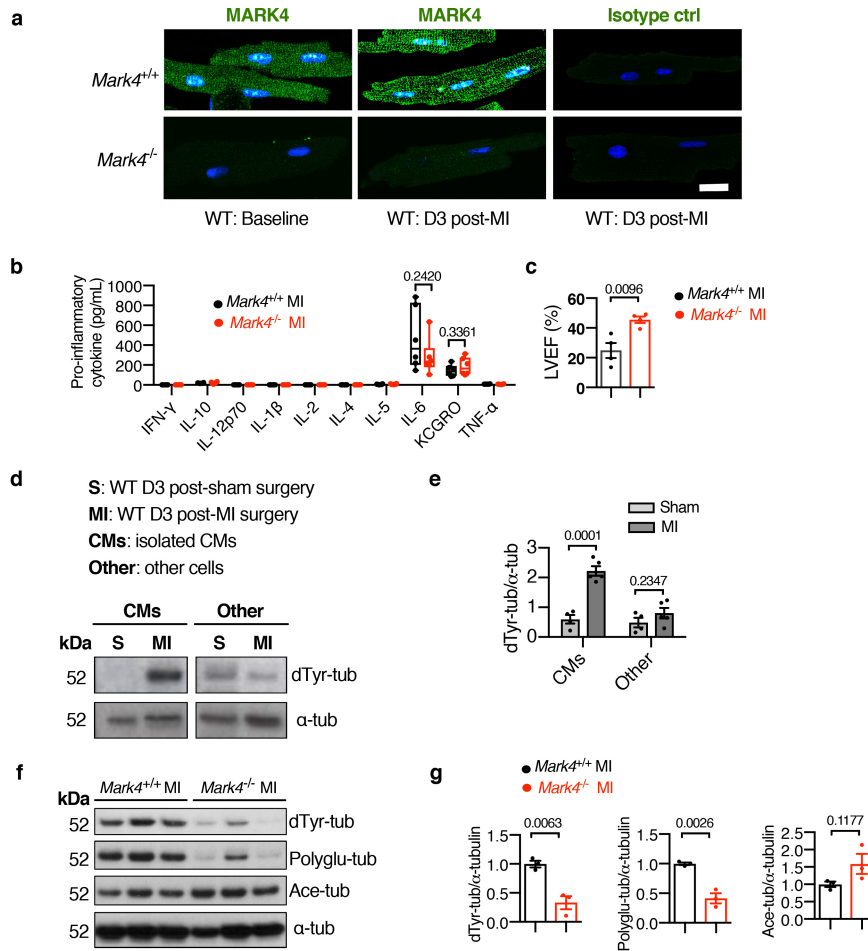
Reprints and permissions information is available at <http://www.nature.com/reprints>.



Extended Data Fig. 1 | Timeline of experimental design. **a**, Timeline of the experimental design for Fig. 1d, e. Investigation of the effect of total MARK4 deficiency on cardiac function using the model of LAD coronary artery ligation to induce myocardial infarction. Echocardiography (Echo) and histological analyses were performed at the indicated time points. **b**, Timeline of the experimental design for Fig. 2a–c. Investigation of the effect of total MARK4 deficiency on cardiac function at 24 h after myocardial infarction. Echocardiography, circulating cardiac troponin and histological analyses were performed at the indicated time point. **c**, Timeline of the experimental design

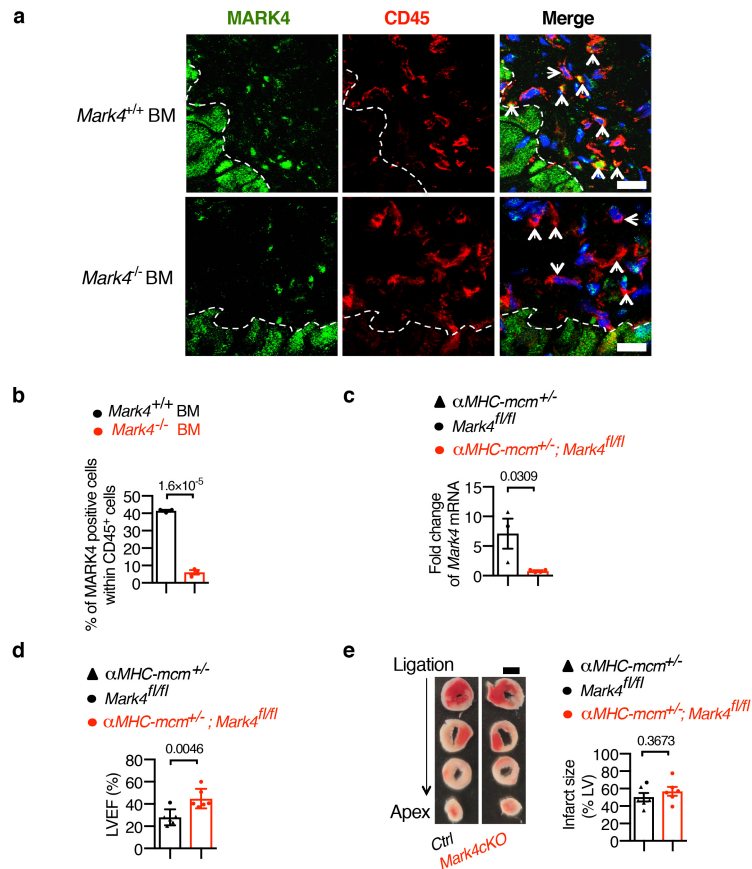
for Fig. 2d and Extended Data Fig. 3a, b. Investigation of the effect of MARK4 expression in haematopoietic cells on cardiac function using the LAD ligation model. BM, bone marrow; BMT, bone marrow transplantation. Echocardiography analysis was performed at the indicated time points.

d, Timeline of the experimental design for Fig. 2e and Extended Data Fig. 3c–e. Investigation of the effect of MARK4 expression in cardiomyocytes on cardiac function using the LAD ligation model. Tm, tamoxifen. *Mark4^{ckO}*, *Mark4* conditional knockout mice. Echocardiography analysis was performed at the indicated time points.



Extended Data Fig. 2 | MARK4 expression, α -tubulin posttranslational modifications and changes in the inflammatory response after myocardial infarction. **a**, Representative confocal images of primary cardiomyocytes (CMs) isolated from *Mark4*^{-/-} or control mice at baseline or at day 3 after myocardial infarction. Scale bar, 20 μ m. **b**, Levels of pro-inflammatory cytokines at day 3 after myocardial infarction ($n=6$ per group). **c**, LVEF at day 3 after myocardial infarction ($n=4$ per group). **d**, **e**, Western blots of detyrosinated α -tubulin in cell lysates of cardiomyocytes isolated from wild-type mice at day 3 after myocardial infarction or post-sham surgery (S), with the lysates of the remaining cells from the same hearts used as control. **f**, Representative western blots. **g**, Ratio of detyrosinated α -tubulin, polyglutamylated α -tubulin or acetylated α -tubulin over total α -tubulin quantified using western blot data from biologically independent samples. Sham group, $n=4$ mice; myocardial infarction group, $n=5$ mice.

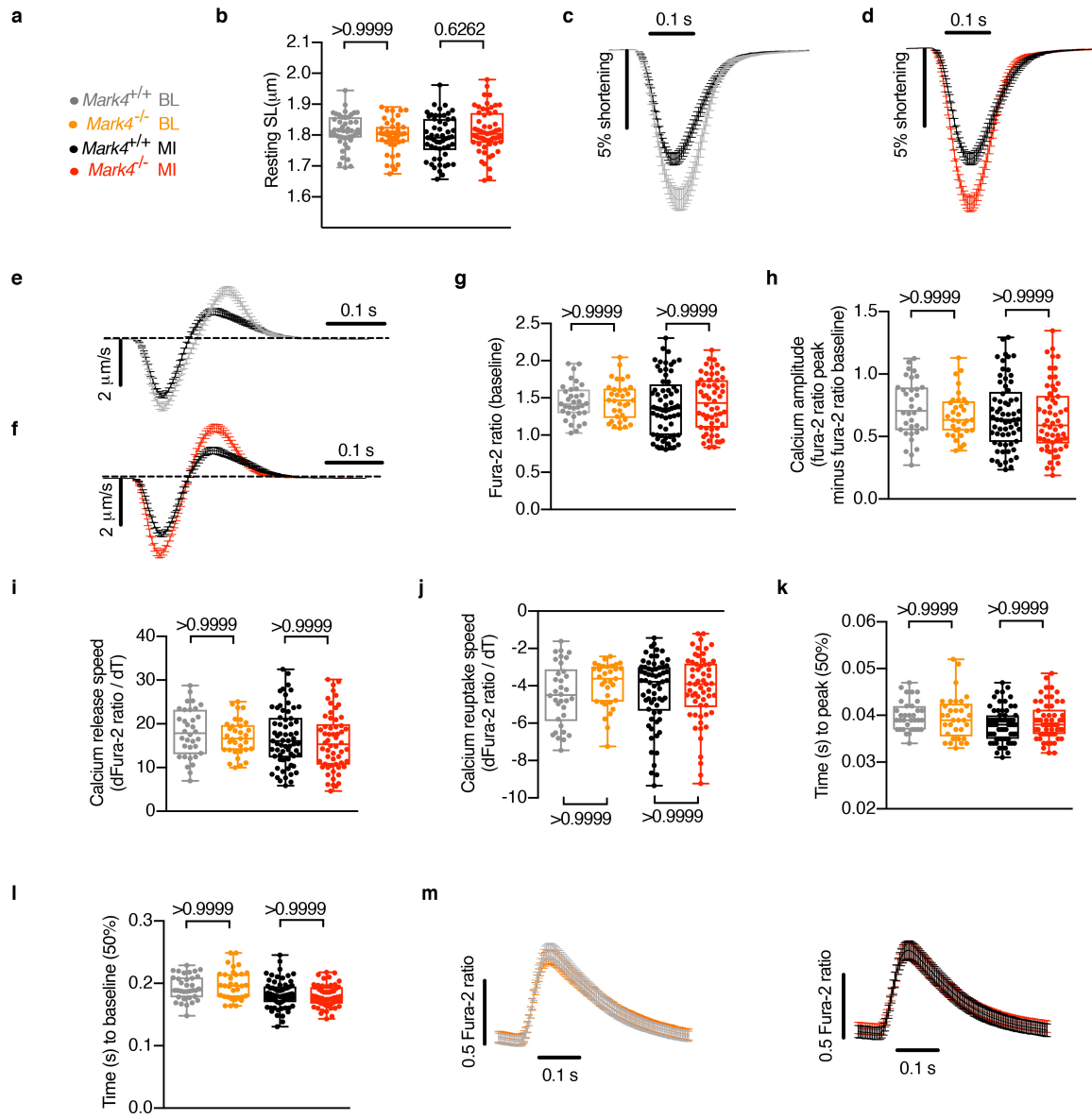
f, g, Western blots of cell lysates from the isolated cardiomyocytes of *Mark4*^{-/-} or control mice at day 3 after myocardial infarction to detect detyrosinated α -tubulin, polyglutamylated α -tubulin (Polyglu-tub), acetylated α -tubulin (Ace-tub) and α -tubulin. **f**, Representative western blots. **g**, Ratio of detyrosinated α -tubulin, polyglutamylated α -tubulin or acetylated α -tubulin over total α -tubulin quantified using western blot data from biologically independent samples ($n=3$ mice per group). **b**, The box bounds represent the 25th and 75th percentiles, the middle line shows the median, the whiskers show the minimum and maximum, and individual replicates are shown as circles. **c, e, g**, Data are mean \pm s.e.m. **b, c, e, g**, Two-tailed unpaired *t*-tests were used; *P* values are indicated.



Extended Data Fig. 3 | Validation of the mouse models for MARK4 selective expression in either haematopoietic cells or cardiomyocytes.

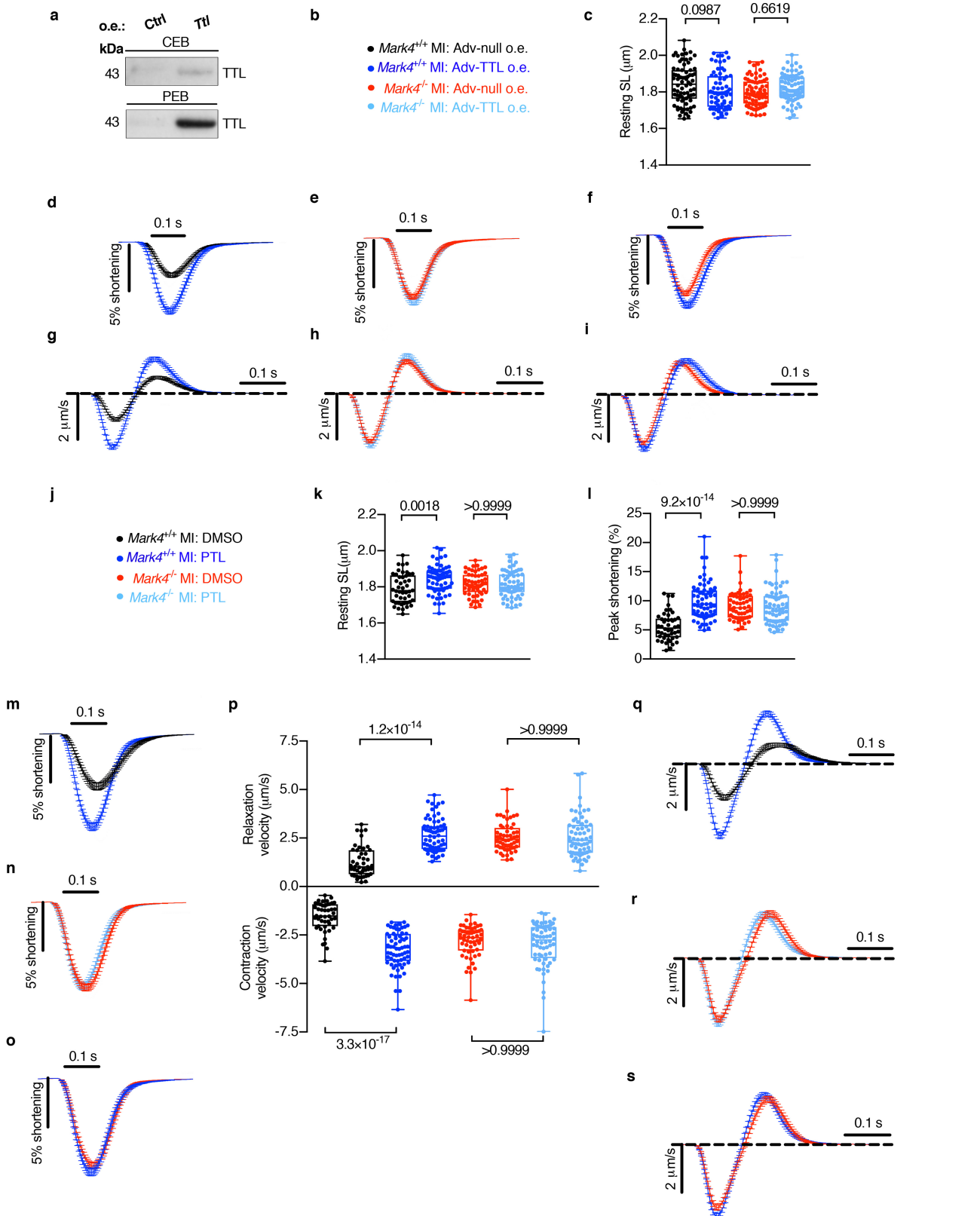
a, b, Confirmation of MARK4 deficiency in CD45⁺ cells of chimeric wild-type mice reconstituted with bone marrow (BM) cells from *Mark4^{-/-}* mice (strategy is shown in Extended Data Fig. 1c). **a**, Representative image with arrows pointing to CD45⁺ cells in the infarct area. Scale bars, 20 μ m (**a**). **b**, Quantification of the percentage of MARK4⁺ cells (green) within CD45⁺ cells (red). $n=3$ mice per group. **c**, Confirmation of *Mark4* deletion in cardiomyocytes (strategy is shown

in Extended Data Fig. 1d). Real-time PCR of *Mark4* level in primary cardiomyocytes isolated from *Myh6-mcm^{+/+};Mark4^{fl/fl}* (also known as α MHC-mcm^{+/+}; *Mark4^{fl/fl}*) ($n=4$) and control mice ($n=3$) at day 7 after the last tamoxifen injection. **d**, Assessment of LVEF of a different group (compared with Fig. 2e) of *Mark4* cKO and control mice ($n=6$ per group) at day 1 after myocardial infarction. **e**, Infarct size at 24 h after myocardial infarction ($n=6$ per group). Scale bar, 2 mm. **b–e**, Data are mean \pm s.e.m.; two-tailed unpaired t-test; P values are indicated.



Extended Data Fig. 4 | The effect of MARK4 deficiency on sarcomere length, peak shortening, velocity and calcium transients in cardiomyocytes before and after myocardial infarction. **a–f**, Contractility assay of single primary cardiomyocytes isolated at baseline or at day 3 after myocardial infarction from the following groups: $\text{Mark}4^{+/+}$ baseline ($n=4$ mice, $n=45$ cardiomyocytes examined over 4 independent experiments), $\text{Mark}4^{-/-}$ baseline ($n=3$ mice, $n=45$ cardiomyocytes examined over 3 independent experiments), $\text{Mark}4^{+/+}$ myocardial infarction ($n=5$ mice, $n=54$ cardiomyocytes examined over 5 independent experiments) and $\text{Mark}4^{-/-}$ myocardial infarction ($n=6$ mice, $n=57$ cardiomyocytes examined over 6 independent experiments). **a**, Colour denotation of samples. **b**, Resting sarcomere length. **c, d**, Average sarcomere shortening traces were compared. **e, f**, Average velocity traces (dSL/dT). **g–n**, Calcium influx assay on single cardiomyocytes isolated from $\text{Mark}4^{-/-}$ or control mice at baseline or at day 3 after myocardial infarction in the

following groups: $\text{Mark}4^{+/+}$ baseline group ($n=2$ mice, $n=34$ cardiomyocytes examined over 2 independent experiments), $\text{Mark}4^{-/-}$ baseline group ($n=2$ mice, $n=33$ cardiomyocytes examined over 2 independent experiments), $\text{Mark}4^{+/+}$ myocardial infarction group ($n=4$ mice, $n=65$ cardiomyocytes examined over 4 independent experiments) and $\text{Mark}4^{-/-}$ myocardial infarction group ($n=3$ mice, $n=58$ cardiomyocytes examined over 3 independent experiments). **g**, Basal Ca^{2+} level. **h**, Amplitude level of Ca^{2+} transients. **i**, Ca^{2+} release speed during contraction. **j**, Ca^{2+} reuptake speed during contraction. **k**, Ca^{2+} elevation time. **l**, Ca^{2+} reuptake time. **m**, Traces of Ca^{2+} kinetic curves. **b, g–l**, The box bounds represent the 25th and 75th percentiles, the middle line shows the median, the whiskers show the minimum and maximum, and individual cardiomyocytes are shown as circles. **b, g–l**, Two-way ANOVA with Bonferroni post hoc correction for multiple comparisons; P values are indicated.

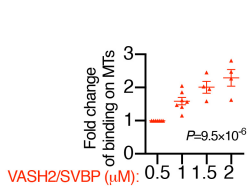
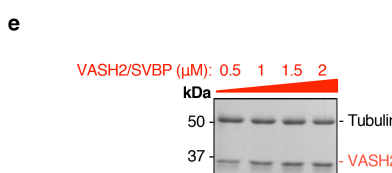
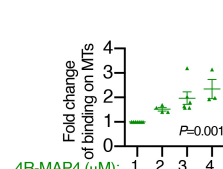
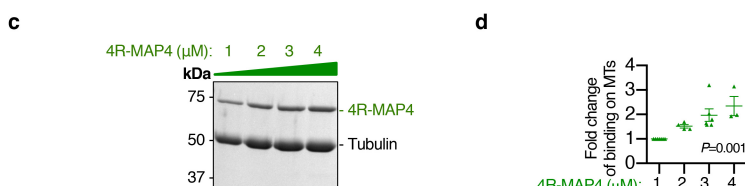
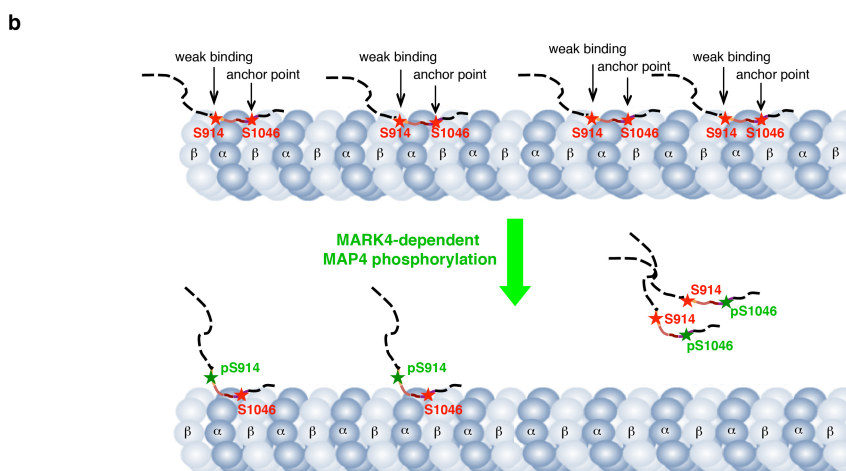


Extended Data Fig. 5 | See next page for caption.

Article

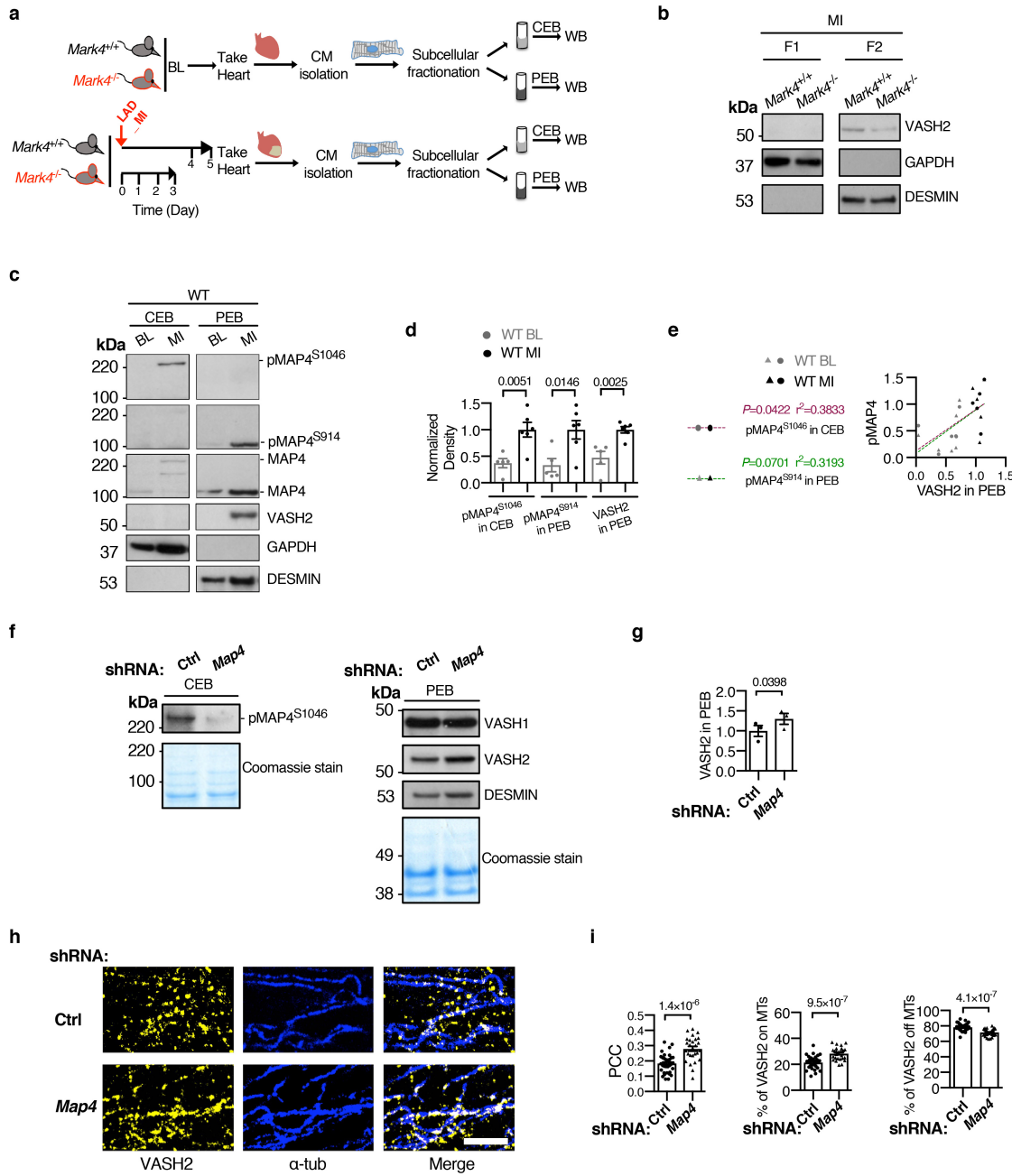
Extended Data Fig. 5 | The effect of TTL overexpression, or PTL treatment, on contractility of *Mark4*^{-/-} cardiomyocytes after myocardial infarction.
a–i, Adenovirus (Adv)-mediated overexpression (o.e.) of TTL in cardiomyocytes isolated from *Mark4*^{-/-} or control *Mark4*^{+/+} mice at day 3 after myocardial infarction, with overexpression of a null vector as control (Ctrl). **a**, Representative western blot. **b–i**, Contractility assay of single cardiomyocytes with overexpression in the following groups: *Mark4*^{+/+} myocardial infarction Adv-Null ($n=3$ mice, $n=75$ cardiomyocytes examined over 3 independent experiments), *Mark4*^{+/+} myocardial infarction Adv-TTL ($n=3$ mice, $n=69$ cardiomyocytes examined over 3 independent experiments), *Mark4*^{-/-} myocardial infarction Adv-Null ($n=3$ mice, $n=74$ cardiomyocytes examined over 3 independent experiments) and *Mark4*^{-/-} myocardial infarction Adv-TTL ($n=3$ mice, $n=73$ cardiomyocytes examined over 3 independent experiments). **b**, Colour denotation of samples. **c**, Resting sarcomere length. **d–f**, Average sarcomere shortening traces. **g–i**, Average velocity traces (dSL/dT). **j–s**, Contractility assay of single cardiomyocytes isolated at day 3

after myocardial infarction with the following treatments: *Mark4*^{+/+} myocardial infarction DMSO ($n=3$ mice, $n=46$ cardiomyocytes examined over 3 independent experiments), *Mark4*^{+/+} myocardial infarction PTL ($n=3$ mice, $n=67$ cardiomyocytes examined over 3 independent experiments), *Mark4*^{-/-} myocardial infarction DMSO ($n=3$ mice, $n=55$ cardiomyocytes examined over 3 independent experiments) and *Mark4*^{-/-} myocardial infarction PTL ($n=3$ mice, $n=64$ cardiomyocytes examined over 3 independent experiments). **j**, Colour denotation of samples. **k**, Resting sarcomere length. **l**, Sarcomere peak shortening. **m–o**, Average sarcomere shortening traces. **p**, Pooled data of contraction velocity and relaxation velocity. **q–s**, Average velocity traces (dSL/dT). **c, k, l, p**, The box bounds represent the 25th and 75th percentiles, the middle line shows the median, the whiskers show the minimum and maximum and individual cardiomyocytes are shown as circles. **c, k, l, p**, Two-way ANOVA test with Bonferroni post hoc correction for multiple comparisons; *P* values are indicated.



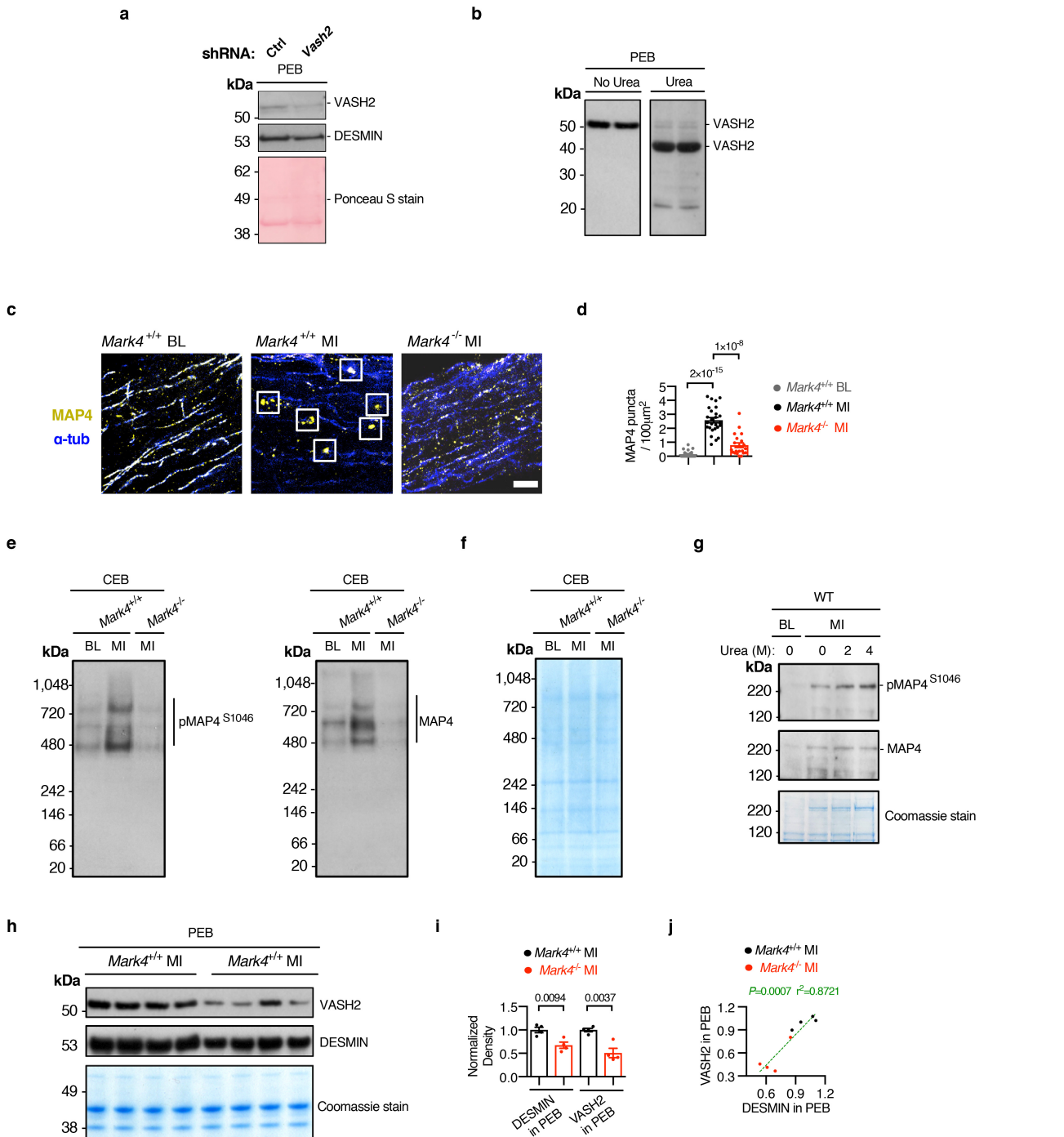
Extended Data Fig. 6 | The association of MAP4 or VASH2 with polymerized microtubules. **a**, Protein sequence alignment between human MAP4 (NP002366) and mouse MAP4 (NP001192259). KXGS motifs (highlighted with red frames) within the tubulin-binding repeats (highlighted with yellow, brown, dark brown and purple frames) of MAP4 are MARK4 substrate sites. S941 of human MAP4 (S914 of mouse MAP4) and S1073 of human MAP4 (S1046 of mouse MAP4) are conserved phosphorylation sites within the KXGS motifs. **b**, Schematic illustration of the possible association between MAP4 and microtubules before or after MARK4-dependent phosphorylation. Unphosphorylated MAP4 binds to microtubules. After MARK4-dependent phosphorylation of S914 of mouse MAP4 at the microtubule weak binding site, MAP4 makes allosteric changes. After MARK4-dependent phosphorylation of S1046 of mouse MAP4 at the microtubule anchor site, MAP4 detaches from

microtubules. **c**, Representative gel image of 4R-MAP4 (1–4 μM) binding to the polymerized microtubules (5 μM) in a microtubule co-sedimentation assay. **d**, Quantification of the binding shown in **c**. $n = 7$ samples examined over 3 independent experiments (1 μM); $n = 4$ samples examined over 3 independent experiments (2 μM); $n = 6$ samples examined over 3 independent experiments (3 μM); $n = 3$ samples examined over 3 independent experiments (4 μM). **e**, Representative gel image of VASH2-SVBP (0.5–2 μM) binding to the polymerized microtubules (2.5 μM) in a microtubule co-sedimentation assay. **f**, Quantification of the binding shown in **e**. $n = 7$ samples examined over 5 independent experiments (0.5 μM); $n = 7$ samples examined over 5 independent experiments (1 μM); $n = 4$ samples examined over 3 independent experiments (1.5 μM); $n = 4$ samples examined over 3 independent experiments (2 μM). **d, f**, Data are mean \pm s.e.m.; one-way ANOVA; P values are indicated.



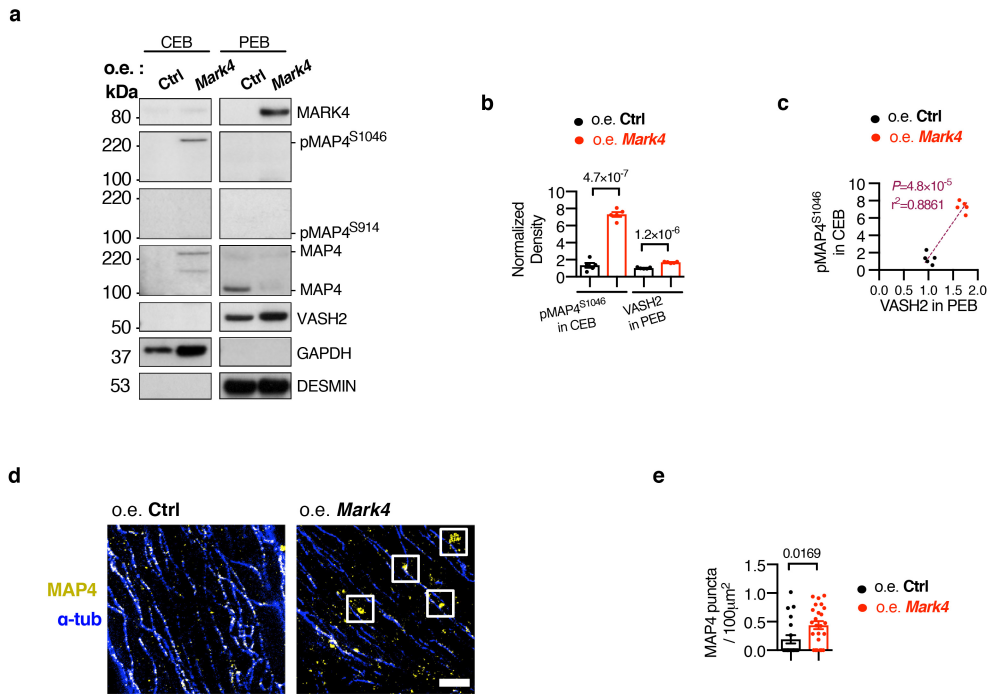
Extended Data Fig. 7 | Association of VASH2 with microtubules in cardiomyocytes before and myocardial infarction, and the effect of MAP4 knockdown. **a**, Subcellular fractionation of primary cardiomyocytes isolated from mice at baseline or after myocardial infarction. Western blotting of the fractions from CEB or PEB. **b**, Representative western blots of the free-tubulin fraction (F1) and extraction from the stable pellet fraction (F2) obtained using a conventional fractionation method. **c–e**, Western blots of CEB or PEB fractions of wild-type (WT) cardiomyocytes at baseline or after myocardial infarction. **c**, Representative western blots (derived from the same experiment). **d**, Quantification of pMAP4(S1046) in CEB, pMAP4(S914) in PEB and VASH2 levels in PEB ($n = 5$ mice at baseline, $n = 6$ mice after myocardial infarction, blots were processed in parallel). **e**, Correlation between VASH2 level in the PEB fraction and pMAP4 levels. **f–i**, Wild-type cardiomyocytes after myocardial

infarction transduced with adenovirus-mediated *Map4* or control shRNA. **f**, Representative western blots of CEB or PEB fraction, and Coomassie-stained gels loaded with the same amounts of proteins. **g**, Quantification of VASH2 levels in PEB ($n = 3$ mice examined over 3 experiments per group). **h, i**, STED images of VASH2 and α-tubulin in the cardiomyocytes after knocking down MAP4. **h**, Representative images. Scale bar, 2 μm. **i**, Pearson correlation coefficient of VASH2 and α-tubulin signals, percentage of VASH2 signals on the polymerized microtubules and percentage of VASH2 signals off the polymerized microtubules, in the following groups: control shRNA ($n = 2$ mice, $n = 35$ cardiomyocytes examined over 2 independent experiments) and *Map4* shRNA ($n = 2$ mice, $n = 27$ cardiomyocytes examined over 2 independent experiments). **d, g, i**, Data are mean ± s.e.m.; two-tailed unpaired *t*-test. **e**, Two-tailed correlation test. *P* values are indicated.



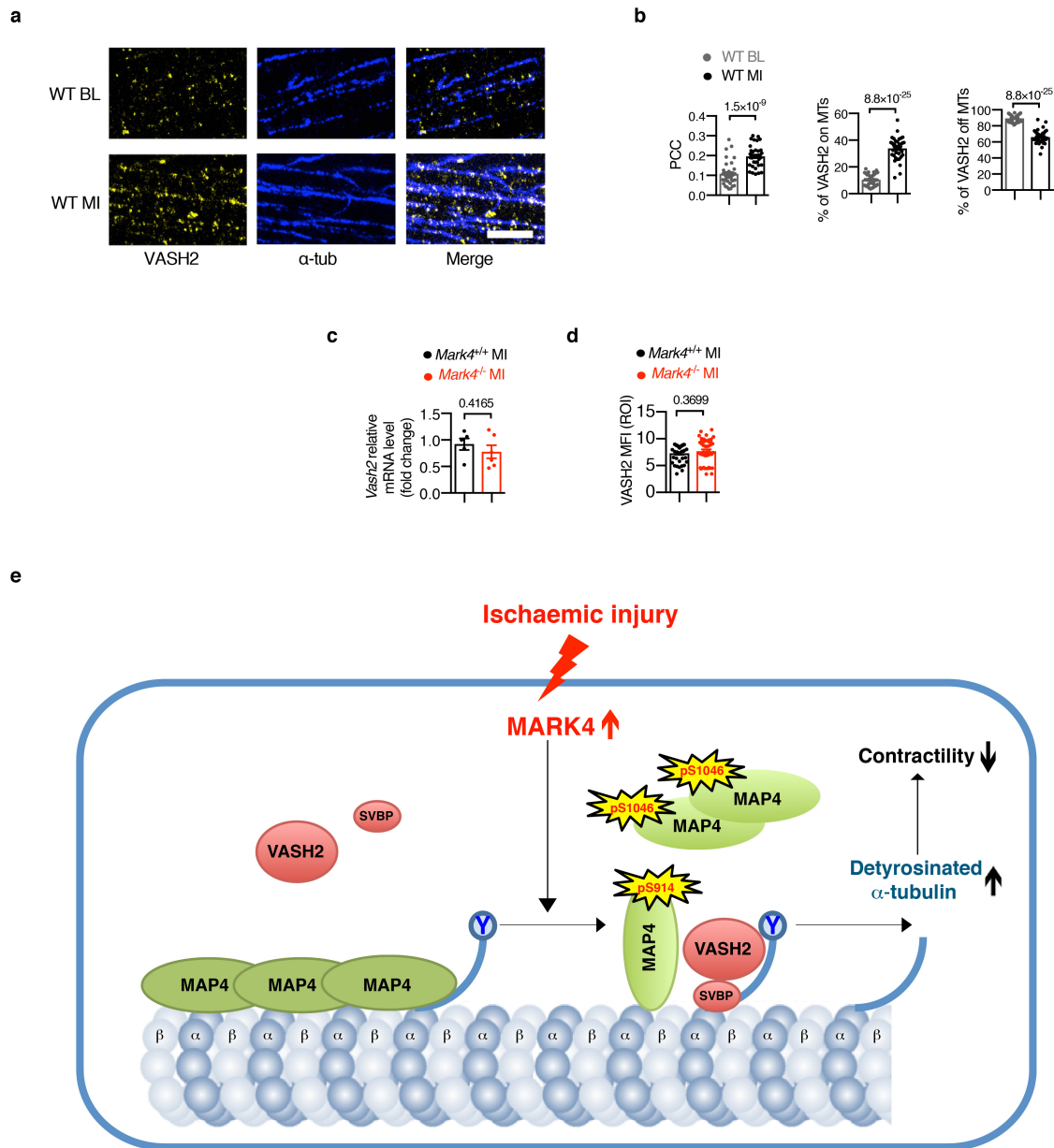
Extended Data Fig. 8 | The status of VASH2 and MAP4 in cardiomyocytes before and after myocardial infarction. **a**, Subcellular fractionation of wild-type cardiomyocytes, isolated from mice after myocardial infarction and transduced with adenovirus-mediated *Vash2* or control shRNA. Representative western blots of fraction in PEB, with the same membrane stained with Ponceau S. **b**, Representative western blot of PEB extractions denatured in the presence or absence of urea from cardiomyocytes after myocardial infarction. **c, d**, STED images of MAP4 and α-tubulin in cardiomyocytes of *Mark4*^{-/-} or control mice at baseline or after myocardial infarction. **c**, Representative images. Oligomerized puncta are indicated within the square frames. Scale bar, 2 μm. **d**, Quantification of the presence of the MAP4 oligomerized puncta in the following groups: *Mark4*^{+/+} baseline ($n=2$ mice, $n=22$ cardiomyocytes examined over 2 independent experiments), *Mark4*^{+/+} myocardial infarction ($n=2$ mice, $n=26$ cardiomyocytes examined over 2 independent experiments)

and *Mark4*^{-/-} myocardial infarction ($n=2$ mice, $n=21$ cardiomyocytes examined over 2 independent experiments). **e, f**, Western blot of native gels loaded with samples in CEB of cardiomyocytes isolated at baseline or after myocardial infarction. **e**, The presence of pMAP4(S1046) and total MAP4 is indicated. **f**, Coomassie-stained native gel loaded with the same amounts of proteins as used in **e**. **g**, Western blot of the CEB fraction denatured in the presence of urea, with a Coomassie-stained denaturing gel loaded with the same amounts of protein. **h**, Western blot of fractions in PEB of cardiomyocytes isolated from *Mark4*^{-/-} or control mice after myocardial infarction, with a Coomassie-stained gel loaded with the same amounts of proteins. **i**, Quantification of VASH2 and desmin levels in PEB fraction ($n=4$ mice per group). **j**, Correlation between desmin and VASH2 levels in PEB. **d, i**, Data are mean \pm s.e.m.; two-tailed unpaired *t*-test. **j**, Two-tailed correlation test. *P*values are indicated.



Extended Data Fig. 9 | MARK4 overexpression regulates MAP4 phosphorylation, and the presence of MAP4 oligomers in the cytosolic fraction. **a–c.** Subcellular fractionation of wild-type cardiomyocytes transduced with adenovirus to overexpress *Mark4* or a null control. **a.** Representative western blots of fractions in CEB or PEB (derived from the same experiment). **b.** Quantification of pMAP4(S1046) in CEB and VASH2 level in PEB ($n = 5$ mice per group, blots were processed in parallel). **c.** Correlation between VASH2 level in the PEB fraction and pMAP4 levels. **d, e.** STED images of

MAP4 and α -tubulin in wild-type cardiomyocytes at baseline transduced with adenovirus to overexpress *Mark4* or a null control. **d.** Representative images. Scale bar, 2 μm . **e.** Quantification of MAP4 oligomerized puncta in the following groups: overexpression of control ($n = 2$ mice, $n = 20$ cardiomyocytes examined over 2 independent experiments) and overexpression of *Mark4* ($n = 2$ mice, $n = 24$ cardiomyocytes examined over 2 independent experiments). **d, e.** Data are mean \pm s.e.m.; two-tailed unpaired *t*-test. **c.** Two-tailed correlation test. *P* values are indicated.



Extended Data Fig. 10 | VASH2 status in cardiomyocytes before and after myocardial infarction, and the schematic summary of the results.

a, b, STED images of VASH2 and α -tubulin in wild-type cardiomyocytes at baseline or after myocardial infarction. **a**, Representative images. Scale bar, 2 μ m. **b**, Pearson correlation coefficient of VASH2 and α -tubulin signals, percentage of VASH2 signals on the polymerized microtubules and percentage of VASH2 signals off the microtubules in the following groups: wild-type baseline ($n = 4$ mice, $n = 38$ cardiomyocytes examined over 2 independent experiments) and wild-type myocardial infarction ($n = 38$ cardiomyocytes of $n = 6$ mice, $n = 38$ cardiomyocytes examined over 3 independent experiments).

c, Real-time PCR of cardiomyocytes after myocardial infarction from the following groups: $Mark4^{+/+}$ myocardial infarction ($n = 5$ mice) and $Mark4^{-/-}$ myocardial infarction ($n = 6$ mice). **d**, Quantification of VASH2 mean fluorescence intensity (MFI) within the cell area (region of interest (ROI)) using

the STED images from the following groups: $Mark4^{+/+}$ myocardial infarction ($n = 6$ mice, $n = 38$ cardiomyocytes examined over 3 independent experiments) and $Mark4^{-/-}$ myocardial infarction ($n = 6$ mice, $n = 47$ cardiomyocytes examined over 3 independent experiments). **e**, Data are mean \pm s.e.m.; two-tailed unpaired *t*-test. *P* values are indicated. **e**, A working model for the MARK4-dependent regulation of microtubule detyrosination after myocardial infarction. After ischaemic injury, increased MARK4 phosphorylates MAP4 at its KXGS motifs. Phosphorylated MAP4 either changes its conformation on the polymerized microtubules or detaches itself from the polymerized microtubules to form oligomerized MAP4 structures in the cytosol. The phosphorylation of MAP4 by MARK4 allows for space access of VASH2 to the polymerized microtubules, thereby promoting α -tubulin detyrosination. As a consequence, the increased level of detyrosinated microtubules causes a reduction in the contractile function of the cardiomyocyte.

Reporting Summary

Nature Research wishes to improve the reproducibility of the work that we publish. This form provides structure for consistency and transparency in reporting. For further information on Nature Research policies, see our [Editorial Policies](#) and the [Editorial Policy Checklist](#).

Statistics

For all statistical analyses, confirm that the following items are present in the figure legend, table legend, main text, or Methods section.

n/a Confirmed

- The exact sample size (n) for each experimental group/condition, given as a discrete number and unit of measurement
- A statement on whether measurements were taken from distinct samples or whether the same sample was measured repeatedly
- The statistical test(s) used AND whether they are one- or two-sided
Only common tests should be described solely by name; describe more complex techniques in the Methods section.
- A description of all covariates tested
- A description of any assumptions or corrections, such as tests of normality and adjustment for multiple comparisons
- A full description of the statistical parameters including central tendency (e.g. means) or other basic estimates (e.g. regression coefficient) AND variation (e.g. standard deviation) or associated estimates of uncertainty (e.g. confidence intervals)
- For null hypothesis testing, the test statistic (e.g. F , t , r) with confidence intervals, effect sizes, degrees of freedom and P value noted
Give P values as exact values whenever suitable.
- For Bayesian analysis, information on the choice of priors and Markov chain Monte Carlo settings
- For hierarchical and complex designs, identification of the appropriate level for tests and full reporting of outcomes
- Estimates of effect sizes (e.g. Cohen's d , Pearson's r), indicating how they were calculated

Our web collection on [statistics for biologists](#) contains articles on many of the points above.

Software and code

Policy information about [availability of computer code](#)

Data collection

VisualSonics Vevo 3100 was used for echocardiography data collection; IonWizard 7.4 was used for Cardiomyocyte contractility and calcium data collection; BD FACSDiva Software 6.0 was used for the flow cytometry data collection; LightCycler480 software release 1.5.0.39 was used for real time PCR data collection; Leica Application Suite Advanced Fluorescence (LAS AF) 2.4.0 build 6254 was used for IHC and histology data collection; Leica Application Suite Advanced Fluorescence (LAS AF) 2.7.3.9723 was used for the confocal microscopy data collection; STED image data were collected with a custom program written in National Instrument (NI) LabVIEW 2014 64-bit, NI FPGA Module and NI Vision Development Module. Custom STED microscope control software used for data collection in this study is available on GitHub and can be accessed online at <https://github.com/Gurdon-Super-Res-Lab/STED-Control>

Data analysis

GraphPad Prism 7.05 and Microsoft Excel (version 2102) was used for statistics data analysis, and GraphPad 9.1.0 (216) was used for violin plots; Vevo LAB3.1.1. was used for echocardiography data analysis; IonWizard 7.4 was used for cardiomyocyte contractility and calcium data analysis; FlowJo (v10) was used for flow cytometry data analysis; Image J (v2.0) was used for western blot band density analysis, histology & IHC image analysis, confocal image analysis, and some of STED image analysis; A customized algorithm, available in GitHub (https://github.com/zhaoaite/dynamic_thresholding_algorithm), was used for STED image analysis.

For manuscripts utilizing custom algorithms or software that are central to the research but not yet described in published literature, software must be made available to editors and reviewers. We strongly encourage code deposition in a community repository (e.g. GitHub). See the Nature Research [guidelines for submitting code & software](#) for further information.

Data

Policy information about [availability of data](#)

All manuscripts must include a [data availability statement](#). This statement should provide the following information, where applicable:

- Accession codes, unique identifiers, or web links for publicly available datasets
- A list of figures that have associated raw data
- A description of any restrictions on data availability

All the associated raw data presented in this paper are available from the corresponding author upon reasonable request. Source data are provided with this paper.

Field-specific reporting

Please select the one below that is the best fit for your research. If you are not sure, read the appropriate sections before making your selection.

Life sciences Behavioural & social sciences Ecological, evolutionary & environmental sciences

For a reference copy of the document with all sections, see nature.com/documents/nr-reporting-summary-flat.pdf

Life sciences study design

All studies must disclose on these points even when the disclosure is negative.

Sample size	Sample sizes for in vivo experiments were based on knowledge of the intra-group variation and pilot conducted experiments in which statistically significant differences were observed between groups. Samples size was also determined as reasonable number of animals allowing statistical analysis while complying with the 3Rs rule on reducing, replacing and refining the use of animals for scientific purpose. The sample size (n) of each experiment is provided in the figure legends.
Data exclusions	Data were excluded if the LAD surgeries failed (mice were not recovered within 24h post-MI or underwent unsuccessful LAD ligation). Outlier exclusion was applied to Masson staining and TTC staining data, and samples with small infarct/scar size less than 35% (due to failed LAD ligation or anatomy variant) were excluded from data. STED images with no good focus on the linear microtubule structures were excluded from the STED image analysis.
Replication	In vivo findings at early time points post-MI were replicated at least 3 times (batches) in independent experiments. All the ex vivo and in vitro experiments were biologically & independently replicated as noted in text, figure legends and methods.
Randomization	All studies were performed with randomization when necessary. Mice were age, gender, genetic background-matched littermates between groups. Mice were randomly assigned prior to surgery, bone marrow transplantation, and other interventions. Cardiomyocytes were randomly selected within each genotype or treatment group in contractility experiments and imaging experiments. Cardiomyocytes were randomly assigned with different treatments or transductions. Randomization does not apply to co-sedimentation assay.
Blinding	Investigators were blinded to the genotypes when performing surgeries, echocardiography measurements, confocal imaging, and STED imaging. All data analysis on above experiments, and histological analysis were conducted in a blinded manner. Measurement of cTnI and inflammatory cytokines were conducted by core facility researchers without knowing the genotypes. Microtubule co-sedimentation assay, real time PCR, and the ex vivo experiments (contractility and calcium measurements, fractionation assays, and western blotting) were not blinded due to logistical issues, but all the procedures and analysis were equal in different groups in those experiments.

Reporting for specific materials, systems and methods

We require information from authors about some types of materials, experimental systems and methods used in many studies. Here, indicate whether each material, system or method listed is relevant to your study. If you are not sure if a list item applies to your research, read the appropriate section before selecting a response.

Materials & experimental systems

n/a	Involved in the study
<input type="checkbox"/>	<input checked="" type="checkbox"/> Antibodies
<input checked="" type="checkbox"/>	<input type="checkbox"/> Eukaryotic cell lines
<input checked="" type="checkbox"/>	<input type="checkbox"/> Palaeontology and archaeology
<input type="checkbox"/>	<input checked="" type="checkbox"/> Animals and other organisms
<input checked="" type="checkbox"/>	<input type="checkbox"/> Human research participants
<input checked="" type="checkbox"/>	<input type="checkbox"/> Clinical data
<input checked="" type="checkbox"/>	<input type="checkbox"/> Dual use research of concern

Methods

n/a	Involved in the study
<input checked="" type="checkbox"/>	<input type="checkbox"/> ChIP-seq
<input type="checkbox"/>	<input checked="" type="checkbox"/> Flow cytometry
<input checked="" type="checkbox"/>	<input type="checkbox"/> MRI-based neuroimaging

Antibodies

Antibodies used

Antibodies applied were described in the relevant sections of on-line method. Antibodies used are listed with information of antibody (including the clone name if suitable), the supplier, the catalog number, the lot number (if available), and dilution applied, as below:

MARK4 Ab, CST, 4834S, 3, 1:1000 WB;
 MARK4 Ab, Abcam, ab12426, GR3197381-5, 1:200 IF, 1:200 IHC;
 Detyrosinated α-tubulin Ab, Abcam, ab48389, GR3309909-1, 1:1000 WB, 1:200 IF;
 α-tubulin Ab (DM1A), CST, 3873S, 12, 1:1000 WB, 1:200 IF, 1:200 STED;
 MAP4 (phospho S1073) Ab, Abnova, PAB15916, 1021, 1:1000 WB;
 MAP4 (phospho S941) Ab, Abcam, ab56087, GR324863-2, 1:1000 WB;
 MAP4 Ab, Abcam, ab245578, GR3259936-1, 1:1000 WB, 1:200 STED;
 VASH1 Ab, Abcam, ab199732, GR3224901-2, 1:1000 WB;
 VASH2 Ab, Abcam, ab224723, GR3199655-27, 1:1000 WB, 1:200 STED;
 GAPDH Ab(D16H11), CST, 5174S, 6, 1:1000 WB;
 DESMIN Ab, R&D, AF3844, YIL0617121, 1:1000 WB;
 TTL Ab, Proteintech, 13618-1-AP, 1:1000 WB;
 Polyglutamylated α-Tubulin Ab (GT335), AdipoGen, AG-20B-0020-C100, A27791601, 1:1000 WB;
 Acetylated α-Tubulin Ab, Santa Cruz Biotechnology, sc23950, C1813, 1:1000 WB;
 Rabbit IgG isotype control, Novus Biologicals, N8810-56910, P120-101-11, 1:1000 IHC, 1:1000 IF;
 APC anti-mouse CD45 Ab (30-F11), BioLegend, 103112, B210891, 1:200 IF, 1:100 FC;
 Brilliant Violet 605 anti-mouse CD3 Ab (17A2), BioLegend, 100237, 1:100 FC;
 FITC anti-mouse CD19 Ab (1D3), Biosciences, 553785, 1:100 FC;
 PE CY7 anti-mouse CD11c Ab (N418), Biolegend, 117318, 1:100 FC;
 AF488 anti-mouse CD11b Ab (M1/70), Biolegend, 101217, 1:100 FC;
 Pacific blue anti-mouse Ly6G Ab (1A8), Biolegend, 127612, 1:100 FC;
 PE anti-mouse F4/80 Ab (BM8), Biolegend, 123110, 1:100 FC;
 Biotinylated anti-rabbit secondary antibody, Abcam, ab6720, 1:800 IHC;
 Atto 594 goat anti-Rabbit IgG, Sigma, 77671, 1:500 STED;
 Atto 647N goat anti-mouse IgG, Sigma 50185, 1:500 STED;
 AF488 donkey anti-rabbit IgG, Invitrogen, A21206, 1981155, 1:200 IF;
 AF647 goat anti-mouse IgG, Invitrogen, A21236, 1654338, 1:200 IF;
 AF647 goat anti-rat IgG; Invitrogen, A21247, 2999156, 1:200 IF;
 Goat Anti-Mouse IgG H&L (HRP), Abcam, ab205719, GR3279214-3, 1:100,000 WB;
 Goat Anti-Rabbit IgG H&L (HRP), Abcam, ab205718, GR3307521-1, 1:100,000 WB;
 Polyclonal rabbit anti goat IgG (HRP), Dako, P0160, 00072616, 1:10,000 WB.

Validation

Antibodies were validated based on information provided by the vendors, as listed below.

MARK4 Ab(CST, 4834S, <https://www.cellsignal.com/products/primary-antibodies/mark4-antibody/4834>) used in WB was validated by the absent detection of specific signals using Mark4-/-samples, and the presence of specific detection with heterologous overexpression of MARK4.

MARK4 Ab (Abcam, ab12426, <https://www.abcam.com/mark4-antibody-ab124267.html>) used in IF & IHC was validated by the absent detection of specific signals using Mark4-/-samples, and by using appropriate IgG isotype control.

VASH2 Ab (Abcam, ab224723, <https://www.abcam.com/vash2-antibody-ab224723.html>) used in WB was validated by using samples with specific knocking-down of VASH2. The antibody used in STED was validated by using appropriate IgG isotype control.

Detyrosinated α-tubulin Ab, <https://www.abcam.com/detyrosinated-alpha-tubulin-antibody-microtubule-marker-ab48389.html>

α-tubulin Ab, <https://www.cellsignal.com/products/primary-antibodies/a-tubulin-dm1a-mouse-mab/3873>

MAP4 (phospho S1073) Ab, http://www.abnova.com/products/products_detail.asp?catalog_id=PAB15916

MAP4 (phospho S941) Ab, <https://www.abcam.com/map4-phospho-s941-antibody-carboxyterminal-end-ab56087.html>

MAP4 Ab, <https://www.abcam.com/map4-antibody-ab245578.html>

VASH1 Ab, <https://www.abcam.com/vash1-antibody-epr17420-ab199732.html>

VASH2 Ab, <https://www.abcam.com/vash2-antibody-ab224723.html>

GAPDH Ab(D16H11), <https://www.cellsignal.com/products/primary-antibodies/gapdh-d16h11-xp-rabbit-mab/5174>

DESMIN Ab, https://www.novusbio.com/products/desmin-antibody_af3844

TTL Ab, <http://www.ptgcn.com/products/TTL-Antibody-13618-1-AP.htm>

Polyglutamylated α-Tubulin Ab (GT335), <https://adipogen.com/storeconfig/choose/store?destination=ag-20b-0020-anti-polyglutamylation-modification-mab-gt335.html>

Acetylated α-Tubulin Ab, https://www.scbt.com/p/acetylated-alpha-tubulin-antibody-6-11b-1?gclid=CjwKCAjwpKCDBhBPEiwAFgBzjzvZolyuC_qgZ7seUiq7PzUOZJM9I2o87g00-yGuH0lw33wovOON2BoCE5AQAvD_BwE

Rabbit IgG isotype control, https://www.novusbio.com/products/igg-isotype-control_nb810-56910

APC anti-mouse CD45 Ab(30-F11), <https://www.biolegend.com/en-us/products/apc-anti-mouse-cd45-antibody-97>

Brilliant Violet 605 anti-mouse CD3 Ab (17A2), <https://www.biolegend.com/fr-fr/products/brilliant-violet-605-anti-mouse-cd3-antibody-8503>

FITC anti-mouse CD19 Ab (1D3), <https://www.bdbiosciences.com/eu/applications/research/stem-cell-research/hematopoietic-stem-cell-markers/mouse/negative-markers/fitc-rat-anti-mouse-cd19-1d3/p/553785>

PECY7 anti-mouse CD11c Ab (N418), <https://www.biolegend.com/ja-jp/products/pe-cyanine7-anti-mouse-cd11c-antibody-3086>

AF488 anti-mouse CD11b Ab (M1/70), <https://www.biolegend.com/en-gb/products/alex-fluor-488-anti-mouse-human-cd11b-antibody-2700>

Pacific blue anti-mouse Ly6G Ab (1A8), <https://www.biolegend.com/en-gb/products/pacific-blue-anti-mouse-ly-6g-antibody-6082>

PE anti-mouse F4/80 Ab (BM8), <https://www.biolegend.com/en-gb/products/pe-anti-mouse-f4-80-antibody-4068>

Animals and other organisms

Policy information about [studies involving animals](#); [ARRIVE guidelines](#) recommended for reporting animal research

Laboratory animals

All mice were on a C57BL/6 background and housed under standard conditions of temperature (18–23°C) and humidity (40–60%) with a 12-hour light/dark cycle. Mark4^{-/-} mice were kindly provided by Prof Yuguan Shi (Barshop Institute), and Mutant Mouse Resource and Research Center (MMRRC, University of California, Davis); αMHC-mcm^{+/+} Cre mice were originally from the Jackson Laboratory; Mark4fl/fl mice were from Taconic Biosciences. αMHC-mcm^{+/+} Cre mice were crossed with Mark4fl/fl mice to generate αMHC-mcm^{+/+} Cre; Mark4fl/fl. All mice were used at eight to ten-week old. Mice used in Fig 1d, 1e, 2a, 2b, 2c, 2d, 2e, and Supplementary table 1 & table 2 are females, both male and female mice were used in the other experiments.

Wild animals

No wild-animals were used in the study.

Field-collected samples

No field-collected samples were used in the study.

Ethics oversight

All experiments were approved by the Home Office, UK, and were performed under PPL PA4BDF775.

Note that full information on the approval of the study protocol must also be provided in the manuscript.

Flow Cytometry

Plots

Confirm that:

- The axis labels state the marker and fluorochrome used (e.g. CD4-FITC).
- The axis scales are clearly visible. Include numbers along axes only for bottom left plot of group (a 'group' is an analysis of identical markers).
- All plots are contour plots with outliers or pseudocolor plots.
- A numerical value for number of cells or percentage (with statistics) is provided.

Methodology

Sample preparation

The method of sample preparation is available in the Methods.

Instrument

FACS LSR II Fortessa (BD Biosciences).

Software

Flow cytometry data were collected using BD FACSDiva Software 6.0, and flow cytometry data were analyzed using FlowJo software (v10).

Cell population abundance

Cardiac CD45+ immune cells were around 0.3–0.8% of the single live cells in sham group, and around 1.3–6% of the single live cells in the MI group; Cardiac CD45+ CD11c high cells were around 2–4% of the CD45+ cells in the sham group, and around 7–16% of the CD45+ cells in the MI group; Cardiac T cells were around 7–20% of the CD45+ cells in the sham group, and

Gating strategy

around 8-38% pf the CD45+ cells in the MI group; Cardiac B cells were around 30-40% of the CD45+cells in the sham group, and around 30-60% of the CD45+ cells in the MI group; Cardiac neutrophils were around 6-8% of the CD45+ cells in the sham group, and around 11-40% of the CD45+ cells in the MI group; Cardiac macrophages were around 8-13% of the CD45+ cells in the sham group, and around 26-50% of the CD45+ cells in the MI group.

The relevant gating strategies are shown in Supplementary Figure 2.

Tick this box to confirm that a figure exemplifying the gating strategy is provided in the Supplementary Information.